X-612-68-12
PREPRINT

PERTURBATIONS OF THE INTERPLANETARY MAGNETIC FIELD BY THE LUNAR WAKE

N. F. NESS
K. W. BEHANNON
H. E. TAYLOR
Y. C. WHANG

JANUARY 1968

GSFC
GODDARD SPACE FLIGHT CENTER
GREENBELT, MARYLAND

X612-68-12

PERTURBATIONS OF THE INTERPLANETARY MAGNETIC FIELD BY THE LUNAR WAKE

N. F. Ness
K. W. Behannon
H. E. Taylor*
Y. C. Whang*

Laboratory for Space Sciences
NASA-Goddard Space Flight Center
Greenbelt, Maryland

January 1968

To be published in Journal of Geophysical Research

*NAS-NRC Resident Postdoctoral Research Associate

PERTURBATIONS OF THE INTERPLANETARY MAGNETIC FIELD BY THE LUNAR WAKE

Abstract

Detailed measurements of the interplanetary magnetic field in the vicinity of the moon have been performed on the Explorer 35 selenocentric spacecraft launched July 1967. The observational evidence fails to reveal the existence of a lunar bow shock wave. A pseudo-magnetosphere as suggested by Gold and interpreted from Luna 10 measurements is not observed. The interplanetary magnetic field appears to be convected through the lunar body without a large scale distortion of its direction or magnitude. Perturbations as much as 30% of the average magnitude are noted in the solar plasma umbra and penumbra. As the satellite passes through the leeward flow an alternating pattern of magnitude increases and decreases is observed in the penumbra while generally only an increase is observed in the umbra. Using a theoretical model of plasma flow due to Whang, a first order solution of the perturbed interplanetary magnetic field is compared with observations. It is concluded that the perturbations can be partially explained on the basis of the magnetization, gradient and curvature currents induced in the disturbed solar plasma flow. The umbral increase and the innermost penumbral decrease are consistent with the first order theory and it is suggested that a higher order approximation is required to explain the newly detected penumbral increases and additional penumbral fluctuations.

Introduction

A previous report (Ness et al., 1967) has presented early results from the NASA-GSFC magnetic field experiment carried on Lunar Explorer 35. This satellite was placed into selenocentric orbit on July 22, 1967 with aposelene = 9388 $\pm$ 100 km (5.4 R_M), periselene = 2568 $\pm$ 15 km (1.5 R_M), period=11.5 hours and initial aposelene-moon-sun angle = 304°. The initial interpretation of these data indicated the absence of a bow shock wave formed in the supersonic flow of solar plasma past the moon. The NASA-GSFC magnetic field experiment does not yet find a bow shock wave across which the interplanetary magnetic field increases abruptly by a factor of 2 to 4 nor the development of a fluctuating magnetic field regime in a sheath layer. In a related study, Lyon et al. (1967) reported the existence of a plasma shadow region behind the moon in which a detectable solar plasma flow was absent. In addition there appeared to be no evidence in these data for a shock wave which would be detectable by the presence of a sheath layer of "hot" electrons and a disturbed proton flux. These results do not support the earlier interpretations of the existence of a lunar magnetosphere from measurements performed by the Luna 10 spacecraft in 1966 (Dolginov et al., 1967).

A feature of the magnetic field observations noted by Ness et al. (1967) and Colburn et al. (1967) was the existence of increases in the interplanetary magnetic field magnitude in the solar wind shadow region and associated decreases of the magnitude in the penumbral region of the solar plasma flow. On the basis of the absence of a large scale disturbance of the interplanetary magnetic field in the flow past the moon, Whang (1967) developed a theory of plasma flow based upon a guiding center approximation. In this model the solar plasma is treated as a

collisionless gas with one dimensional thermal motion of the protons only along magnetic field lines. A long non-axially symmetrical wake region is developed behind the moon in which a plane of symmetry exists defined by the local solar wind velocity and interplanetary magnetic field direction. The exact geometry of the wake depends upon both the direction of the interplanetary magnetic field and the thermal energy of the protons, i.e., the ratio of the mean random velocity of the solar plasma to its bulk velocity.

It is the purpose of this paper to present additional observational evidence supporting the original conclusions by Ness et al. (1967) on the absence of a detectable shock wave and to study in detail the perturbations of the interplanetary magnetic field in the lunar wake. These measurements will then be compared with theoretical results based upon the Whang model of the solar plasma flow. The perturbations are due to magnetization, gradient and curvature currents in the disturbed solar plasma flow. Studies of the solar plasma flow around the moon have been conducted by Michel (1967 a,b) and Johnson and Midgley (1967) and their relation to the present study shall be discussed.

The data to be presented in this report cover only the interval from July 29 - August 6, 1967. These data follow shortly after those discussed in the earlier publication by Ness et al. (1967) and represent an interval of time during which the moon's position relative to the earth changes from third quarter to new moon. During this time interval RF shadowing of the spacecraft is restricted to near the time of aposelene and a continuous monitoring of the interplanetary magnetic field in the leeward portion of the lunar wake is possible. Analysis

of data obtained from subsequent orbits leads to the same conclusions reached from a detailed study of this limited interval of data. As will be seen there exists a variety of new observational features, most of which fit into a coherent pattern of small perturbations.

Data Analysis

Details of the NASA-GSFC magnetic field experiment on Explorer 35 have been presented in the previous publication by Ness et al. (1967). A particularly interesting but also complicating aspect of the spacecraft system has been its performance in the optical shadow of the moon. In the absence of a solar input, all directional references on the spacecraft would be lost were it not for the inclusion of a pseudo-sun pulse which provides a timing reference signal through the lunar shadow. The time interval between successive sun pulses during the lunar shadow is equal to the last spin period obtained in solar illumination. If the spacecraft rotation rate remained constant through lunar shadow then this would provide a reasonable estimate for computation of directional references.

An intrinsic feature of the spacecraft, however, is that in lunar shadow the rotation rate increases, due to thermal contraction and the conservation of angular momentum. As the spacecraft loses the heat input from the sun it is cooled and contracts. This contraction decreases the angular moment of inertia and hence the spacecraft rotation rate must increase. As the spacecraft emerges from lunar shadow the process is reversed and the spacecraft de-spins to its original rotation rate.

The net change in rotation period throughout this optical shadow, of generally 30 to 40 minutes in length, is only (a few) about one part in a thousand, actually 2 parts in 1837. However, during the 30 minute interval, with a nominal 2.29 second spin period, the slight change is sufficient so that directional measurements at the end of the optical

shadow are in error by 360^{o} or more due to the cumulative effects during the more than 1000 rotations of the satellite.

A detailed study of this phenomenon and a numerical-analytical technique for rectification of directional measurements in the optical shadow of the moon has been conducted by Taylor (1967). In this paper experimental results are presented in which directional references have been corrected for the variable spin rate of the spacecraft both in optical shadow and thereafter. The accuracy of the correction procedure is estimated at $\pm 10^{o}$. It may be noted that this correction is applied only to the azimuthal angle, ϕ, so that none of the directional uncertainty is present in the latitudinal angle, θ.

While in the direct solar illumination directional measurements are limited by the sensitivity and accuracy of the instrument ($\pm$ .1γ and $\pm$ 0.3γ, respectively) and the accuracy with which the spin axis orientation itself is known ($\pm 2^{o}$). In a typical interplanetary magnetic field of 6 gamma the sensitivity uncertainty leads to a directional uncertainty of $\pm 1^{o}$. Thus for all the measurements reported here, magnitudes are presented with an accuracy of $\pm$ 0.3γ and directions are presented with an uncertainty of less than 3^{o} while the spacecraft is in sunlight, but perhaps as much as 10^{o} during the optical shadow.

Experimental data to be reported are the sequence averages in selenocentric solar ecliptic coordinates computed from nominally 16 measurements at 5.12 second intervals. Computation of the RMS deviation of both the magnitude (δF) and the separate components (δC) has been included. The magnitude and component deviations are defined as

$$\delta F = \left[\frac{1}{N}\sum_{i=1}^{N}(F_i - \langle F\rangle)^2\right]^{\frac{1}{2}} \qquad (1)$$

and

$$\delta C = \left\{\frac{1}{N}\sum_{i=1}^{N}\left[(B_{xi} - \langle B_x\rangle)^2+(B_{yi} - \langle B_y\rangle)^2+(B_{zi} - \langle B_z\rangle)^2\right]\right\}^{\frac{1}{2}}$$

$N \leq 16$. These two quantities are particularly diagnostic in a study of the solar wind interaction with the moon for they are sensitive to the existence of a sheath region in which fluctuating magnetic fields would be readily identified. Note that $\delta C \geq \delta F$ always.

The relative geometry of the satellite orbit has been shown in Figure 2 of the earlier publication of Ness et al. (1967). The data to be presented in this paper cover the interval from July 29-August 6 and the relative orbital parameters are changed only slightly in a selenocentric solar ecliptic system, the aposelene-moon-sun angle decreasing from $\phi_{SSE} = 290^{o}$ to 284^{o}. Since the orbital plane of the satellite is inclined at 169^{o} to the selenocentric solar ecliptic equatorial plane, i.e., almost parallel, the three dimensional positional reference can reasonably be approximated by the selenocentric solar ecliptic longitude (ϕ_{SSE}) and the selenocentric distance RAD as measured in units of lunar radii (1 R_M = 1738.1 km). For interpretation of the results, the position of the orbit relative to the previously defined "plane of symmetry" is also important.

The data to be presented are final production data from which possible noise points have been eliminated. The threshold criteria used to delete a particular average field vector are

(i) $\delta C/F > .33$ and $\delta C \geq .95$ or
(ii) more than 20% of the individual measurements used in computing the average are missing, i.e. $N \leq 12$.

There are also obvious gaps in the data plots which correspond to

periods when the spacecraft is in the range and range rate mode. No scientific data is transmitted during these intervals, of approximately 10 minutes (8 sequences). The ranging mode was scheduled frequently when the spacecraft was approximately 90° in azimuth from the moon-sun line, $\phi_{SSE} = 90^{\circ}$.

Experimental Observations

In Figure 1 the results are shown for 2 orbital passes in late July when the moon was in the interplanetary medium. In the upper half of the figure the interplanetary magnetic field magnitude is observed to be perturbed in a very characteristic manner. As the spacecraft approaches the lunar optical shadow there is a small increase from 7.5γ to 8.5γ in the magnetic field at 1610 UT on July 29 followed by a decrease to 6.5γ and then a much broader increase to approximately 8.7γ in the optical shadow. Several data points are missing thereafter but a decreased field is readily identified followed by an increased field. Then the interplanetary field returns to near its preshadow value in both direction and magnitude.

It is to be noted that the perturbations of the magnetic field magnitude in this example are clearly identified as a characteristic pattern of a short dipolar + -, a longer +, and finally a short dipolar - + anomaly with + and - representing an increase and decrease, respectively. The magnetic field perturbations are about a gamma in an average field of 7.5γ, a perturbation of less than 20%. Note that the angular deviation of the field direction measured by θ appears to be no more than about 20^{o}, while there appears to be a slight characteristic variation in the azimuthal direction ϕ from pre to postshadow.

The lower half of Figure 1 displays an additional traverse through the lunar wake on July 30 in which the sharply defined features discussed above are not identified. While a rather broad decrease is

observed both pre and postshadow, a shadow increase is not clearly detected. A unique pattern of the θ perturbation in the shadow is noted. The fluctuations of the interplanetary magnetic field as measured by the parameters δC and δF are different in these two passes but the orientation (θ, ϕ) is approximately the same. However, there is no evidence for the existence of a lunar associated region in which the magnetic field suddenly increases at a shock surface and an onset of increased fluctuations is observed. For the relative position of the spacecraft orbit, a shock wave would be expected to be observed between the region defined by $\phi_{SSE} = 135^{o}$ to $\phi_{SSE} = 45^{o}$.

In Figure 2 are represented successive orbital passes on August 1 in which the general pattern of fluctuations or perturbations in the lunar wake is somewhat different than shown in Figure 1. In Figure 2a, it is noted that there is a general increase of the magnetic field throughout the perturbed wake region although there still exists a suggestion of the characteristic + - + - + perturbation pattern. Clearly, the penumbral dipolar anomalies are not as well developed as in Figure 1a. The apparent increase in magnetic fluctuations in the lunar wake during this interval, as measured by δC, is somewhat unique and generally not a characteristic feature of the observations.

In Figure 2b, the well developed + - dipolar perturbation in the solar plasma penumbra is observed on entry but the remainder of the lunar wake region is almost lacking of characteristic perturbations detected previously. No identifiable umbral increase is noted.

In Figure 3 are presented the 2 orbital passes on August 2 in which the readily identifiable dipolar anomalies in the solar plasma

penumbras are present although the time interval and position relative to the optical shadow are different. In Figure 3a, the relative increase in the lunar shadow of the magnetic field between 0110 and 0140 is very small. In Figure 3b, the well-developed dipolar penumbral anomaly is readily identified near 1230 while the perturbation to the interplanetary magnetic field in the solar plasma umbra is missing any increase generally being less than $\frac{1}{2}\gamma$. Here the fluctuations of the magnetic field, as measured by δC and δF, are seen to be extremely low and it is inferred that this time interval represents a period during which the interplanetary medium was very steady and uniform over a three hour interval. No evidence is found for a detached bow shock wave, in this, or indeed in any of these data.

In Figure 4 are presented two successive sets of results obtained on August 3 and 4. The data in Figure 4a display the characteristic patterns of + - + - + perturbations found previously. Note here that the perturbations are similar to those previously obtained with readily identifiable increases preceding the decreases in the solar plasma penumbra.

A classic example of the perturbation of the interplanetary magnetic field by the lunar wake is shown in Figure 4b. The characteristic feature of a + - + - + anomaly is clearly observed. In addition, there appear to be additional + - and - + perturbations identifiable exterior to those noted in the preshadow data.

Additional observations obtained on August 4 and 5 are shown in Figure 5 which reveal the wide variety of perturbations of the interplanetary magnetic field observed in the lunar wake. In Figure 5a

it is seen that the leading anomalies in the solar plasma penumbra are much broader than previously observed but that the perturbation postshadow is quite different in that it is observed for a much shorter time interval. In Figure 5b there appears to be an absence of the characteristic penumbral dipolar perturbations previously observed.

In Figure 6 are shown the last two experimental sets of observations to be presented, obtained on August 5 and 6. The characteristic + - +- + pattern of perturbations is again observed in both orbital passes.

To summarize these experimental observations we note the following: generally there is an increase in magnitude of the interplanetary magnetic field detected in the solar plasma umbral shadow of the moon of up to about 3γ. A relative decrease of up to 4γ is frequently noted on either side of the umbral shadow increase. These decreases generally occur in or near the penumbral plasma shadow of the moon and are bounded on the exterior by additional increases in the magnitude of the field. Thus the characteristic anomalies in the penumbral regions consist of an exterior increase and an interior decrease on either side of the umbral increase. The penumbral dipolar anomalies are not symmetrical in their magnitude or time length as observed by the spacecraft. This is interpreted to represent a feature related to the selenocentric orbit in which the preshadow penumbral anomalies are observed at a radial distance of approximately 2.5 R_M while the postshadow dipolar anomalies are observed at only 1.6 R_M. In addition the spacecraft is moving more slowly at the greater radial distance and this distorts the apparent length and extent of the anomaly. The perturbations observed pre-optical shadow generally extend into the optical shadow period.

A unique feature of these data is that the pre and postshadow perturbations of the interplanetary magnetic field consist not only of a decrease but also an increase of the field. Moreover, on several occasions there is an indication that additional increases and decreases exist further out from the umbra. The development of a pattern of alternating increases and decreases is evident in the data obtained in the solar plasma penumbra. Usually they appear in paired form, i.e., always a preshadow + and - while postshadow they appear as - +. In all cases the magnitude of the anomalies decreases rapidly as the order of the pattern increases. In many instances only the innermost dipolar anomalies are readily identified.

Induced Electric Currents and Associated Magnetic Fields

In order to calculate the perturbations of the interplanetary magnetic field in the lunar wake, it is necessary to know the electric currents in the plasma. In this sector these currents and the perturbations of the interplanetary magnetic field are discussed theoretically. A first order solution of Maxwell's equations has been obtained which approximates a self-consistent solution for the field and the currents. This solution explains both the increase of magnetic field in the umbra and a decrease in the penumbra. It also suggests the presence of periodic increases and decreases outside the umbra.

The variation of the magnetic field is governed by Maxwell's equations

$$\nabla \cdot \underset{\sim}{B} = 0 \tag{2}$$

and

$$\nabla \times \underset{\sim}{B} = \frac{4\pi}{c} \underset{\sim}{J}. \tag{3}$$

Introducing a vector potential $\underset{\sim}{A}$ such that $\underset{\sim}{B} = \nabla \times \underset{\sim}{A}$, and requiring that $\nabla \cdot \underset{\sim}{A} = 0$, then we have

$$\nabla^2 \underset{\sim}{A} = -\frac{4\pi}{c} \underset{\sim}{J} \tag{4}$$

Once the distribution of current density in the lunar wake is known, equation (4) can be solved for $\underset{\sim}{A}$ and thus $\underset{\sim}{B}$ obtained.

In this study three sources of current are considered; the magnetization current, the gradient drift current and the curvature drift current. The magnetization current is produced by the gyration

of the plasma particles in the magnetic field and its density, $\underset{\sim}{J}_M$, may be expressed as

$$\underset{\sim}{J}_M = - \underset{\sim}{\nabla} \times \left(\frac{Nc}{B} < \mu > \underset{\sim}{B} \right) \tag{5}$$

Here $< \mu >$ denotes the average magnetic moment and N the number density of charged particles. Due to a gradient in the magnetic field or a curvature of the field lines, particles of opposite charge will drift in opposite directions. These drifts produce the gradient drift current, $\underset{\sim}{J}_G$, and the curvature drift current, $\underset{\sim}{J}_R$. They may be expressed as

$$\left.\begin{aligned} \underset{\sim}{J}_G &= \frac{Nc}{B^2} < \mu > \underset{\sim}{B} \times \underset{\sim}{\nabla} B \\ \text{and} \\ \underset{\sim}{J}_R &= \frac{P_{\parallel} c}{B^2} \underset{\sim}{B} \times (\underset{\sim}{b} \cdot \underset{\sim}{\nabla} b) \end{aligned}\right\} \tag{6}$$

where

$$P_{\parallel} = \int m v_{\parallel}^2 f d \underset{\sim}{v}$$

is the pressure along the lines of force and $\underset{\sim}{b}$ the unit vector in the direction of the magnetic field. Thus the total electric current in the lunar wake is taken to be

$$\underset{\sim}{J}_{MGR} = \underset{\sim}{J}_M + \underset{\sim}{J}_G + \underset{\sim}{J}_R$$

and equation (3) becomes

$$\begin{aligned} \underset{\sim}{\nabla} \times \underset{\sim}{B} &= \frac{4\pi}{c} \underset{\sim}{J}_{MGR} \\ &= \frac{4\pi}{c} \left(\underset{\sim}{J}_M + \underset{\sim}{J}_G + \underset{\sim}{J}_R \right) \end{aligned} \tag{7}$$

Substituting (5) into (7) yields

$$\nabla \times \left[\left(1 + \frac{4\pi N}{B} <\mu>\right) \underset{\sim}{B}\right] = \frac{4\pi}{c} \left(\underset{\sim}{J}_G + \underset{\sim}{J}_R\right) \tag{8}$$

Since the magnetic moment $<\mu>$ is an adiabatic invariant, the left-hand side of (8) can be expanded into three terms:

$$\left(1 + \frac{4\pi N}{B} <\mu>\right) \nabla \times \underset{\sim}{B} - \frac{4\pi}{B} <\mu> \underset{\sim}{B} \times \nabla N + \frac{4\pi N}{B^2} <\mu> \underset{\sim}{B} \times \nabla B \tag{9}$$

The third term in (9) is identically equal to $\frac{4\pi}{c} \underset{\sim}{J}_G$ and hence shows that equation (8) can be reduced to

$$\nabla \times \underset{\sim}{B} = \frac{4\pi}{B + 4\pi N <\pi>} \underset{\sim}{B} \times \left[<\mu> \nabla N + \frac{P_{\parallel}}{B} \underset{\sim}{b} \cdot \nabla \underset{\sim}{b}\right] \tag{10}$$

Thus the density of induced current in the lunar wake can be expressed as

$$\underset{\sim}{J}_{MGR} = \frac{c}{B + 4\pi N <\mu>} \underset{\sim}{B} \times \left[<\mu> \nabla N + \frac{P_{\parallel}}{B} \underset{\sim}{b} \cdot \nabla \underset{\sim}{b}\right] \tag{11}$$

The average magnetic moment $<\mu>$ can be expressed in terms of B_o/N_o as

$$<\mu> = \frac{\beta B_o}{8\pi N_o}$$

where β is the ratio of the perpendicular pressure to the magnetic pressure in the plasma flow upstream of the moon. For representative values of $T_\perp = 10^4 - 10^5\ ^oK$, $n = 2\text{-}5\ p/cm^3$, $B = 4\text{-}7$ gamma in the interplanetary medium, β is of the order of unity.

In the lunar wake, the electron density can deviate from the ion density only very slightly because of electrostatic forces. The ion flow in the wake region has been studied by Whang (1967). In his model the flow of magnetized solar wind plasma in the vicinity of the moon is treated as a free particle flow in the guiding center limit. In order to write his solution of ion density distribution in selenocentric solar ecliptic coordinates we consider that the solar wind velocity is along the heliocentric radial direction ($-X_{SSE}$) and the interplanetary field upstream is parallel to the plane of the ecliptic, the X-Y plane. The flow field is symmetrical about the Z = 0 plane. The motion of each guiding center particle is restricted to a Z = constant plane. The presence of the moon does not perturb the flow conditions in the region $|Z| > R_M$. Dividing the perturbed flow into three regions as shown in Figure 7, the density distribution, N, and the parallel pressure, $P_{\parallel}$, can be expressed as

$$
\begin{aligned}
&\text{in region I} \quad N = (N_o/2)\ \mathrm{erfc}\ (\gamma_1 S) \\
&\qquad P_{\parallel} = P_{\parallel o}\left[N/N_o + \sqrt{\pi}\ \gamma_1 S \exp(-\gamma_1^2 S^2)\right] \\
&\text{in Region II} \quad N = (N_o/2)\ \mathrm{erfc}\ (\gamma_2 S) \\
&\qquad P_{\parallel} = P_{\parallel}\left[N/N_o + \sqrt{\pi}\ \gamma_1 S \exp(-\gamma_2^2 S^2)\right] \\
&\text{in region III} \quad N = (N_o/2)\left[\mathrm{erfc}\ (\gamma_1 S) + \mathrm{erfc}(\gamma_2 S)\right] \\
&\qquad P_{\parallel} = P_{\parallel o}\left[N/N_o + \sqrt{\pi}\ \gamma_1 S \exp(-\gamma_1^2 S^2) + \sqrt{\pi}\ \gamma_2 S \exp(-\gamma_2^2 S^2)\right]
\end{aligned}
\tag{12}
$$

where

$$\gamma_1 = \sin(\alpha + \lambda)/\sin(\phi - \alpha - \lambda)$$

$$\gamma_2 = \sin(\alpha - \lambda)/\sin(\phi + \alpha - \lambda)$$

$$\alpha = \arcsin\left[(R_M^2 - Z^2)^{\frac{1}{2}}\,(X^2 + Y^2)^{-\frac{1}{2}}\right]$$

$$\lambda = \arctan(Y/X)$$

and

$$S = U/(2k\,T_{\parallel}/M_i)^{\frac{1}{2}}$$

Here $T_{\|}$ represents the average component of the thermal velocity of the ions parallel to the interplanetary magnetic field. The density and the parallel pressure are functions of the speed ratio, S, and the direction angle of the undisturbed magnetic field ϕ.

Since S is the ratio of the solar wind velocity to the ion thermal velocity parallel to the field lines it can vary considerably in the interplanetary medium. For solar wind velocities of 300 to 500 km/sec, a temperature of $2 \times 10^{4}\,^{o}K$ implies speed ratios of 16.7 to 27.7 while for the same range of solar wind velocities and a temperature of $2 \times 10^{5}\,^{o}K$ the speed ratios range from 5.4 to 12.5 respectively. Thus typical values of S range from about 5 to 30. Because higher temperatures are usually found at the times of higher velocities a value of S = 10 is taken to be representative of normal solar wind conditions, based on the speed ratio of the ions only.

Representative lunar wake models resulting from application of (12) are shown in Figure 8 for speed ratios 4 and 10. The interplanetary magnetic field is assumed to be oriented at the theoretical spiral angle of $\phi = 135^{o}$ at 1 AU. It is seen that a large speed ratio leads to a longer and more narrow wake region. The projection of the sample Explorer 35 trajectory in Figure 8 has been chosen in the middle of the time interval covered by the experimental data discussed in the previous section. Whang (1967) has shown that the surfaces of constant ion density and flux are very close to being spatially coincident. Thus for the remainder of this paper, we shall discuss the lunar wake in terms of the density contours since they are explicitly related to the induced electric currents.

In this figure and in the subsequent discussion the umbra of the solar wind plasma shadow is defined as that region behind the moon for which the density value is below a particular threshold selected. In the case of the data shown here the value $N = .01\ N_o$ or 1 percent of the unperturbed density has been chosen. With this definition the length of the umbra in the case S = 4, $\emptyset = 135^o$ is seen to be 3 R_M while in the case S = 10, $\emptyset = 135^o$ the length is about 8 R_M.

The length of the lunar umbra depends critically not only upon the speed ratio S but also field orientation $\emptyset$. In Figure 9 is shown a parametric set of curves yielding the length of the lunar plasma umbra, depending upon the threshold flux level chosen, as a function of speed ratio S and field orientation ϕ. This figure illustrates the essential features of the lunar wake dependency upon field orientation. The shortest umbra is obtained when the field is oriented perpendicular to the solar wind flow ($\phi = 90^o$); an infinitely long umbra would be obtained for field lines parallel to the flow ($\phi = 180^o$). Intermediate lengths are obtained for $90^o < \phi < 180^o$ with the length of the umbra being a sensitive function of both field orientation as well as speed ratio S.

Considerable symmetry exists in the theoretical solution of solar wind flow past the moon. This can be noted by observing that the sense of the field line at a given direction is unimportant. Thus the ion density contours shown in Figure 8 are equally valid for a field orientation of $\phi = 315^o$ ($= 180^o + 135^o$). In addition, the solution can also be considered valid for a field orientation of $\phi = 45^o$ (360^o -

315^{o}) or 225^{o} (360^{o} - 135^{o}) if the selenocentric solar ecliptic coordinate system is rotated about the X axis so that Z is now directed southward to the ecliptic plane. Relative positions of a satellite traversal of the lunar wake would be correspondingly rotated.

Using the induced current density, ion density and parallel pressure given above (Equations (11) and (12)), numerical solutions of equation (4) for the perturbation of magnetic field on the ecliptic are obtained by an iteration process for various values of $p_{\parallel o}/p_{\perp o}$, S, ϕ, and β. The numerical method employed is discussed in detail by Whang (1968).

Numerical solutions for various values of $p_{\parallel o}/p_{\perp o}$ (the ratio of parallel pressure to perpendicular pressure in the unperturbed solar wind) will be discussed first. The measured values of $p_{\parallel o}/p_{\perp o}$ vary from 1.5 to 4 under relatively quiet conditions (Hundhausen et al., 1967). Specific numerical solutions for S = 10, $\phi = 135^{o}$ and $\beta = 1$ are presented in Figure 10 at two radial distances ($R = 2.5\ R_M$ and $R = 4.5\ R_M$). The parameter $p_{\parallel o}/p_{\perp o}$ measures the relative importance of the curvature drift current, J_R/J_{MGR}. From this figure it can be seen that the curvature drift does enhance the magnitude of the magnetic field perturbation, but the general features of the field perturbation remain unchanged. This indicates that the important features of the field perturbation are actually controlled by the magnetization current $\underset{\sim}{J}_M$, and the gradient current $\underset{\sim}{J}_G$ (probably the effect of $\underset{\sim}{J}_G$ is itself small compared to that of $\underset{\sim}{J}_M$). Letting $\underset{\sim}{J}_{MG}$ denote the sum of $\underset{\sim}{J}_M$ and $\underset{\sim}{J}_G$, equation (10) shows that

J_{MG} is proportional to $\underset{\sim}{B} \times \nabla N$. On the plane of symmetry $\underset{\sim}{J}_{MG}$ is perpendicular to that plane but points in opposite directions on either side of the shadow. The magnetic field induced by $\underset{\sim}{J}_{MG}$ causes the increase of magnetic field in the umbra and the decreases in the penumbra.

Specific solutions for $p_{\|o}/p_{\perp o} = 3$, S=7, $\beta = 1$ and R = 3.5 R_M are presented in Figure 11 for three values of ϕ, 105^o, 135^o and 165^o. The noticable effect associated with the varying field orientation may be understood as follows. In the regions where the magnitude of ∇N is relatively large, the vector ∇N is nearly perpendicular to the direction of the solar wind. When the acute angle between the field line and the solar wind direction decreases, J_{MG} increases. Increasing J_{MG} causes both larger increases and larger decreases of the magnetic field in the wake region as shown in Figure 11. Also the length of the umbra changes with ϕ so that at a fixed distance from the moon the relative position in the lunar wake depends on ϕ. Thus at a distance of R = $3.5R_M$, the scale distances of the three solutions shown in Figure 11 are 3.5/4.0 =.88, 3.5/7.8 = .45 and 3.5/14. = .25. It is seen that the largest anomaly is obtained for the smallest scale distance or equivalently for the largest ϕ. Note that there are indications in the bottom curve of relative magnitude increases exterior to the penumbral decreases, as well as variations within the umbra.

Numerical solutions for different speed ratios (S = 4 and 10) at two radial distances (R = 2 R_M and R = 4 R_M) are plotted in Figure 12. From this figure we can see that the variations of the magnitude perturbations are small for different speed ratios <u>if</u> the field orientation is held constant. In this figure it may be noted that the two decreased regions of the penumbra become narrower and closer to each

other as the speed ratio S increases. The reason for this is that as S increases, the wake becomes narrower and the plasma density changes over a narrower region. The effect becomes more apparent as the scale distance R increases.

In the results presented in Figure 13 the effect of varying β on the perturbation of the magnetic field can be seen. The three curves for $\beta = 0.5$, 1, and 2 are nearly similar to one another, and the magnitude of perturbations is approximately linearly proportional to the β values. As $\beta \to 0$, which corresponds to $<\mu> = 0$, the trivial solution of equation (10) is that $\underset{\sim}{B} = \underset{\sim}{B}_o$ everywhere and the interplanetary field will not be perturbed by the lunar wake. Once a solution is obtained for the perturbation of magnetic field for $\beta = 1$, this similarity relation may be used to estimate the magnitude of perturbations for other β values. That is, denoting by B_1 the total field magnitude for the case $\beta = 1$ and by B_o the unperturbed interplanetary value

$$B = B_o + \varkappa\beta\ (B_1 - B_o).$$

Where $\varkappa$ is found to be approximately 0.90.

Qualitatively and quantitatively these theoretical calculations do produce some of the features observed in the satellite data. The following section will discuss the relation of the calculations to the measurements.

Discussion of Results

It has been shown in the previous section that a first order solution of the perturbed interplanetary magnetic field in the lunar wake displays characteristic umbral and penumbral anomalies similar to those experimentally observed. The magnitude of the umbral increases are theoretically predicted to be on the order of 10 to 40 percent. These magnitude anomalies are in good agreement with experimental observations. The innermost penumbral decreases theoretically predicted are less by a factor of 2 to 4 but experimental observations indicate they are of approximately the same magnitude as the umbral increases. Finally the experimental evidence reveals the existence of exterior penumbral increases whose effects are about the same as the umbral increase and the penumbral decreases. Only in the extreme case of the field orientation approximately parallel to the solar wind velocity, as shown in the bottom of Figure 11, has a small penumbral increase been predicted. It is believed that the failure of the present model to adequately explain the penumbral dipolar anomalies is related to its approximate nature.

The solutions which are obtained by Whang (1968) are approximate and valid only in the symmetry plane of the magnetized plasma flow around the moon. As previously noted the induced electric currents are not axially symmetric. Thus if the satellite passes through the lunar wake at various angles with respect to the plane containing the magnetic field and the solar wind velocity vector, the magnetic perturbations observed would be expected to be different. Indeed the first order perturbation theory based upon the zeroth order model of the lunar wake suggests that the narrowest penumbral

anomalies are expected to be observed as the satellite passes through a plane perpendicular to this symmetry plane. The broadest anomalies would be observed in the symmetry plane itself with intermediate orientations and positions yielding intermediate cases between these two extremes.

An attempt has been made in the presentation of the experimental data to consider this fact. In the upper right hand corner of each of the satellite traverses shown in Figures 1-6 is the satellite orbital trace projected into the Y-Z plane. The Z axis is selected perpendicular to the symmetry plane which is defined in terms of the average preshadow interplanetary magnetic field orientation and the moon-sun line. Without direct measurements of the interplanetary plasma flow velocity this symmetry plane is only approximate but should be valid within approximately 10^{o}. In addition the interplanetary magnetic field is observed to fluctuate over a similar range and hence the diagrams only indicate approximate relative positions. The arrow plotted represents the trace of the satellite orbit through the optical shadow with the tail corresponding to the point of entry into the shadow and the head corresponding to the point of exit from the shadow.

As can be noted in Figures 1-6 only a very few cases satisfy the requirement of the satellite trajectory being approximately in the symmetry plane of plasma flow around the moon. However, in several of the cases shown the field is nearly parallel to the moon-sun line so that the wake is nearly axially symmetric. For those cases near the plane of symmetry or with axial symmetry it is possible to directly compare the results with theory. Certain parameters are still unknown

however, namely the speed ratio, S, and the value of β. In a further attempt to interpret the experimental measurements the appropriate value of the planetary magnetic activity index Kp is included in Figures 1 through 6. It is known that high values of Kp generally correspond to increased values of solar plasma velocity, implying a large speed ratio, S. Unfortunately, the relationship of the solar plasma temperature to the activity index Kp is not yet known. However, unless the temperature increases much more rapidly with Kp than does U_o, it is still reasonable to assume that in fact S itself will increase because of the square root dependency of S on $T_{||}$.

A review of the experimental results in the light of the discussion of the satellite motion relative to the symmetry plane and the magnetic activity index leads to the following conclusion. As the Kp index increases the width of the wake region through which the satellite passes appears to decrease if due regard is given to the satellite motion relative to the symmetry plane. More precise comparisons of the theoretical model presented herein and the observed interplanetary magnetic field perturbations will require the introduction of specific plasma parameters defining the speed ratio and the β value for the plasma.

In the work of Colburn et al. (1967), it has been suggested that the increases and decreases of magnetic field in the lunar wake can be explained by means of the equation

$$\frac{B^2}{8\pi} + n\,k\,T_{\perp} = \text{constant} \qquad (13)$$

This describes the balance of total plasma and field pressure in a direction transverse to the magnetic lines of force. In general the magnetic field is not parallel to the direction of the wake, the magnetic field stress is a tensor quantity, and its magnitude is quite different from $B^2/8\pi$ in a direction other than transverse to the lines of force. Specifically the magnetic field exerts a tension of magnitude $B^2/4\pi$ directed along the lines of force as well as a pressure.

The argument by Colburn et al. (1967) that the penumbral decrease of B is due to an increase of $T_\perp$ implies that the magnetic moment is not conserved in the wake region. The use of an expansion fan model of the penumbral decreases in the work by Johnson and Midgley (1967) and Michel (1967b) is based upon the assumption that the solar plasma behavior in the wake is described by a fluid flow model.

In the work presented in this paper, Maxwell's equations are solved directly so that the tensile stress is not ignored. It is suggested here that the induced electric currents due to diamagnetism of the plasma, the gradient drift and the curvature drift are the primary mechanisms disturbing the interplanetary magnetic field in the wake region. Furthermore, since the model is based on the independent motion of particles in their self consistent fields, collective effects such as a tail shock predicted by Michel (1967a,b) are not expected. Thus far the experimental results give no evidence for a tail shock.

When comparing the GSFC magnetometer data with that published by Colburn et al. (1967) from the ARC magnetometer experiment the sharp decrease to 5.3γ shown in their Figure 3 near 1425 UT

on July 31 is not observed. (See Figure 14). From 1415-1430, the NASA-GSFC experiment measures a 6.9γ magnitude average, which is approximately 0.5γ less than the ARC value while the weakest field measured is 6.5γ. It would appear that the ARC data for this particular interval include some spurious data points not eliminated in their analysis. The associated physical interpretations are inapplicable.

One particular advantage of the physical model proposed here is its ability to numerically predict the penumbral increases and decreases experimentally observed so clearly. It is suggested that the penumbral variations be viewed as periodic structures which arise from the gradient of plasma density in the disturbed flow field around the moon. The first order solutions produce primarily decreases in the penumbra but suggest a periodic structure in some cases. Further iteration may be expected to produce both increases and decreases as the self-consistent solution is approached. Work is presently in progress along these lines and will be reported in the future.

In this study, the explicit effect of the induced electric fields in the wake region has been assumed to be negligible. If this is not valid, however, there will not be major differences in the solar wind flow pattern or magnetic field perturbations. The principal effect would be for the electrons, which have a much lower speed ratio, S_e, to attempt to fill in the lunar umbra faster than the ions. The resultant electric field would force the ions to fill in the umbra faster than predicted based upon their own speed ratio, S_i. Thus, the net result is to require the computation of an effective speed ratio, S^*

$$S_e \ll S^* < S_i$$

which is lower than S_i, for determining the geometry of the lunar wake. In the absence of direct measurements of the solar wind electron temperature, T_e, this would then indicate a way of estimating T_e from the discrepancy between the observed wake geometry and the wake predicted using a speed ratio S_i based only upon ion temperatures. However, as noted in the results presented in Figure 12, this may not be a sensitive method to measure T_e since the perturbed interplanetary magnetic field differs only slightly from a value of S=10 to S=4.

An important feature of the observed magnetic perturbations in the lunar wake is their variability. Sometimes they are quite prominent while at other times they are too small to identify. For instance in Figure 1a the increases and decreases are readily identified while in 1b they are quite vague. Similarly the passes in Figure 2, particularly 2a, show very small amplitude changes with only a hint of the characteristic + - + - + behavior.

These changes in the amplitude of the magnetic perturbations are related to the parameter β. As $\beta \rightarrow 0$, the amplitude of the perturbations also vanishes. Thus it is expected that the period from July 30 to August 1 was one of small β and that both before and after this time the plasma energy density was greater. Future comparison with the data from the MIT plasma probe should verify this point. Ultimately it is planned that measurements of both S and β will be used to compute the magnetic perturbations for the purpose of comparing with the magnetometer measurements.

Summary

Repeated measurements from selenocentric orbit by the Lunar Explorer 35 NASA-GSFC magnetic field experiment give no evidence for the existence of a lunar bow shock wave or a standing shock behind the moon. The interplanetary magnetic field appears to be convectively transported through the moon with little distortion and hence the theoretical model proposed by Gold (1966) and interpreted by the Luna 10 measurements (Dolginov et al., 1967) is not supported. Variations of the magnitude of the magnetic field show solar plasma umbral increases of approximately 10 to 30 percent with periodic variations of similar magnitude in the solar plasma penumbra. Variations of the direction of the magnetic field are generally less than 20° - 30°. A characteristic pattern of the magnitude anomalies is + - + - + with the interior + representing the umbral increase and the exterior + - and - + representing the periodic (here dipolar) variations in the penumbra.

From the joint experimental and theoretical results obtained thus far, it appears that the magnetic field perturbations in the lunar wake are of complex geometry depending critically upon the solar wind velocity, density and temperature as well as the field orientation, ϕ. The speed ratio, S, measures the relative magnitudes of the solar wind velocity and thermal ion velocity parallel to the field line and is a critical dimensionless parameter employed in the analysis. The parameter β is also critical.

It is tempting to conclude that higher order iterations of the plasma and field equation will lead to a more self-consistent solution and thus will provide better agreement with observations. At present the absence of definitive plasma data precludes exact comparisons of the experimental

results for those few existing cases in which the satellite orbit is approximately in the symmetry plane of plasma flow. The changing nature of the interplanetary medium on both short and long time scales precludes a statistical study. As additional experimental data are obtained and in particular, from simultaneous observations of the interplanetary medium, by separate satellites a more comprehensive comparison with theory will be possible.

It is suggested that the periodic nature of the field oscillations in the lunar wake are characteristic of the disturbed plasma flow around the moon. On the basis of these results and the theoretical model presented, it is not expected that a tail shock will be observed in the lunar wake, as proposed by Michel (1967a,b).

Acknowledgements

We are indebted to our colleagues Mr. C. S. Scearce and Dr. S. C. Cantarano for their important participation in this experiment. In addition, fruitful discussions of the solar plasma observations with Drs. E. F. Lyons and H. S. Bridge of MIT are greatly appreciated. Discussions with Dr. F. S. Johnson are also appreciated.

References

Colburn, D. S., R. G. Currie, J. D. Mihalov and C. P. Sonett, Diamagnetic Solar Wind Cavity Discovered Behind Moon, Science 158, 1040-1042, 1967.

Dolginov, Sh. Sh., Ye. G. Yeroshenko, L. N. Zhuzgov, and I. A. Zhulin, Possible Interpretation of the Results of Measurements in the Near Lunar Satellite AMS Luna 10, Geomagnetizm i Aeronomiya, 7, 436-441, 1967. (In Russian).

Gold, T., The magnetosphere of the moon, in The Solar Wind, edited by R. J. Mackin, Jr., and N. Neugebauer, pp. 381-392, Pergamon Press, New York, 1966.

Hundhausen, A. J., S. J. Bame, and N. F. Ness, Solar Wind Thermal Anisotropies: Vela 3 and IMP 3, J. Geophys. Res., 72, 5265-5274, 1967.

Johnson, F. and J. E. Midgley, Note on the Lunar Magnetosphere, preprint, 1967.

Lyon, E. F., H. S. Bridge, J. H. Binsack, Explorer 35 Plasma Measurements in the Vicinity of the Moon, J. Geophys. Res., 72, 6113-6117, 1967.

Michel, F. C., Shock Wave Trailing the Moon, J. Geophys. Res., 72, 5508-5509, 1967a.

Michel, F. C., Magnetic Field Structure Behind the Moon, preprint, 1967b.

Ness, N. F., The Magnetohydrodynamic Wake of the Moon, J. Geophys. Res., 70, 517-534, 1965.

Ness, N. F., K. W. Behannon, C. S. Scearce, S. C. Cantarano, Early Results from the Magnetic Field Experiment on Lunar Explorer 35, J. Geophys. Res., 72, 5769-5778, 1967.

Taylor, H. E., Aspect Determination in Lunar Shadow on Explorer 35, NASA-GSFC preprint X-612-67-611, 1967.

Whang, Y. C., Interaction of the Magnetized Solar Wind with the Moon, NASA-GSFC preprint X-612-67-580, 1967.

Whang, Y. C., Theoretical Study of the Magnetic Field in the Lunar Wake, NASA-GSFC preprint X612-68-17, 1968.

FIGURE CAPTIONS

Figure 1 Magnetic field measurements, presented in selenocentric solar ecliptic coordinates, obtained on July 29 and 30, 1967, by Explorer 35. Perturbations of the interplanetary magnetic field identified as relative increases (+) and relative decreases (-) are indicated above the magnitude results. The K_p index of terrestrial magnetic activity for 29 July was 3+ 4- 3- 1+ 0+ 2- 2 4, and for 30 July was 4+ 5 5- 1+ 1 0+ 1- 0+ See text.

Figure 2 Magnetic field measurements, presented in selenocentric solar ecliptic coordinates obtained on August 1, 1967 by Explorer 35. The K_p index of terrestrial magnetic activity for 1 August was 1- 1- 0+ 2- 1 2- 1+ 0+.

Figure 3 Magnetic field measurements, presented in selenocentric solar ecliptic coordinates obtained on August 2, 1967, by Explorer 35. The K_p index of terrestrial magnetic activity for 2 August was 0+ 0+ 0 1+ 0+ 0+ 0+ 1+.

Figure 4 Magnetic field measurements, presented in selenocentric solar ecliptic coordinates, obtained on August 3 and 4, 1967, by Explorer 35. The K_p index of terrestrial magnetic activity for 3 August was 0 0+ 0+ 0+ 1 1 1 2 and on 4 August was 1 1- 2+ 1 3 3 2+ 2-.

Figure 5 Magnetic field measurements, presented in selenocentric solar ecliptic coordinates, obtained on August 4 and 5, 1967 by Explorer 35. The K_p index of terrestrial magnetic activity for 5 August was 3+ 1+ 1+ 2 2+ 2+ 2+ 2- 1. See Figure 4 caption for K_p values on 4 August.

Figure 6 Magnetic field measurements, presented in selenocentric solar ecliptic coordinates, obtained on August 5 and 6, 1967, by Explorer 35. The Kp index of terrestrial magnetic activity on August 6 was 1- 2 1 + 2 1 1 - 2+ 2+. See Figure 5 caption for Kp values on August 5.

Figure 7 Representation of characteristic regions of perturbed plasma flow surrounding moon (Whang, 1967).

Figure 8 Projection of orbit of Explorer 35 on ecliptic plane in lunar wake. The interplanetary magnetic field is assumed to lie in the ecliptic plane at an angle of 135^{o} to the earth-sun-line. Contour lines of uniform density at intervals of N = 0.01, 0.1, 0.5, 0.9 and 0.99 of the undisturbed flow field N_o are presented. U represents the umbral and P the penumbral regions in the flow field assuming a threshold of N = 0.01 N_o and 0.99 N_o.

Figure 9 The length of the lunar wake, defined by the fraction of free stream density N/N_o, as a function of the magnetic field orientation, $\emptyset$. Two families of curves are shown corresponding to the two speed ratios S = 4, 10.

Figure 10 Theoretical perturbed interplanetary magnetic field, F, relative to free stream value F_o in the symmetry plane at R/Rm = 2.5 and 4.5 for S = 10, $\emptyset = 135^{o}$ and $\beta = 1$. Different solutions for $p_{\parallel o}/p_{\perp o} = 2$ and 5 are compared with the solution for $\underset{\sim}{J}_R = 0$.

Figure 11 Theoretical perturbed interplanetary magnetic field, F, relative to free stream value F_o in the symmetry plane at $R/R_M = 3.5$ for $S = 7$, $\beta = 1$, and three values of $\emptyset$.

Figure 12 Theoretical perturbed interplanetary magnetic field F, relative to free stream value F_o and direction $\emptyset$ in symmetry plane for $\emptyset = 135^o$, $\tilde{\beta} = 1$ and $R/R_M = 2$ and 4. Different solutions for speed ratios of 4 and 10 are indicated. The symmetry of these solutions is indicated.

Figure 13 Theoretical perturbed interplanetary magnetic field F, relative to free stream value F_o in the symmetry plane at R/Rm = 1.7 and 4.0 for $S = 7$, $\emptyset = 135^o$ and $p_{\|o}/p_{\perp o}=2$. Different solutions for $\beta = 0.5$, 1 and 2 are indicated.

Figure 14 Magnetic field measurements, presented in selenocentric solar ecliptic coordinates, obtained on July 31, 1967 by the NASA-GSFC experiment on Explorer 35. The Kp index of terrestrial magnetic activity for July 31 was 0+ 0+ 0+ 0 0+ 0+ 0+ 0+.

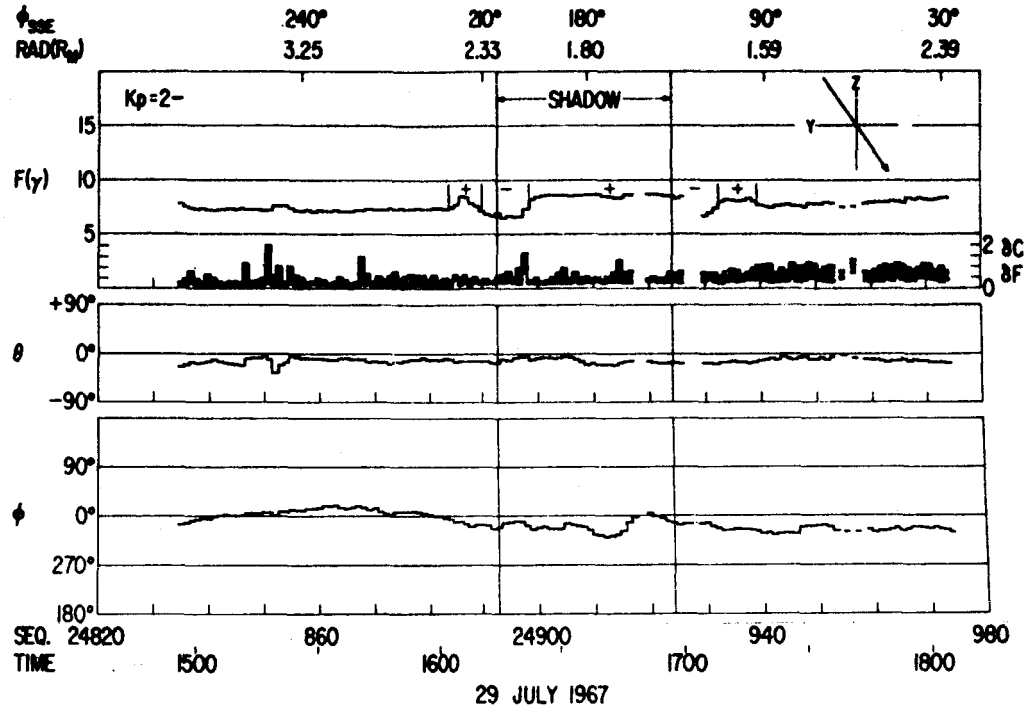
ϕ_{SSE} 240° 210° 180° 90° 30°
RAD(R_M) 3.25 2.33 1.80 1.59 2.39
Kp=2-
SHADOW
Z
Y
15
F(y) 10
5
2 δC
0 δF
+90°
θ 0°
-90°
90°
φ 0°
270°
180°
SEQ. 24820 860 24900 940 980
TIME 1500 1600 1700 1800
29 JULY 1967

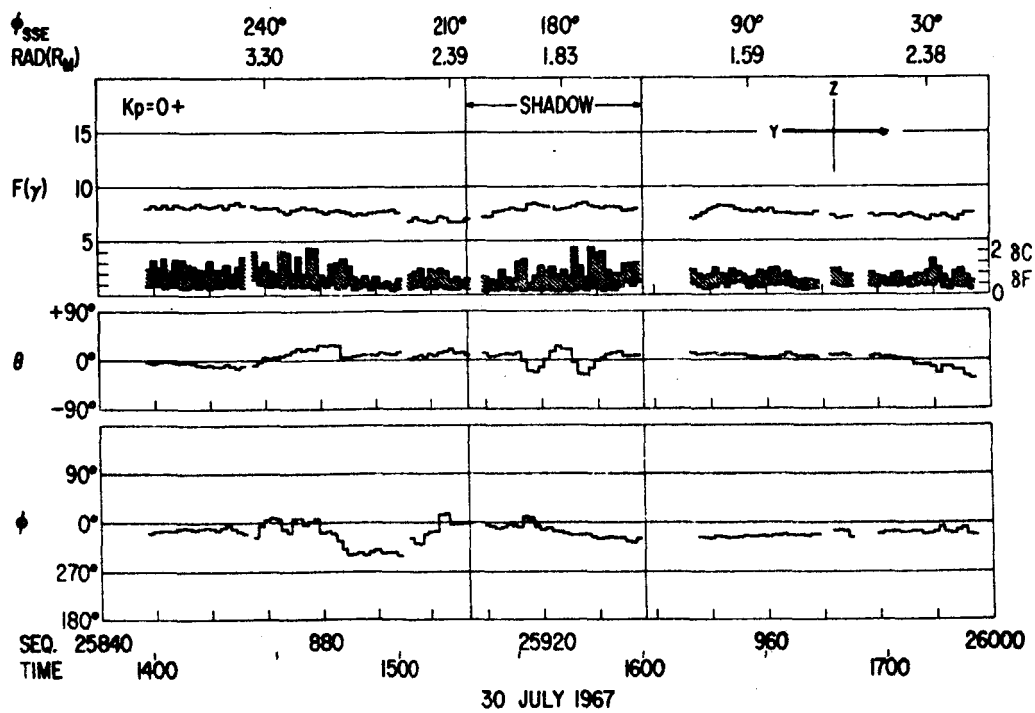
ϕ_{SSE} 240° 210° 180° 90° 30°
RAD(R_M) 3.30 2.39 1.83 1.59 2.38
Kp=0+
SHADOW
Z
Y
15
F(y) 10
5
2 δC
0 δF
+90°
θ 0°
-90°
90°
φ 0°
270°
180°
SEQ. 25840 880 25920 960 26000
TIME 1400 1500 1600 1700
30 JULY 1967

Figure 1

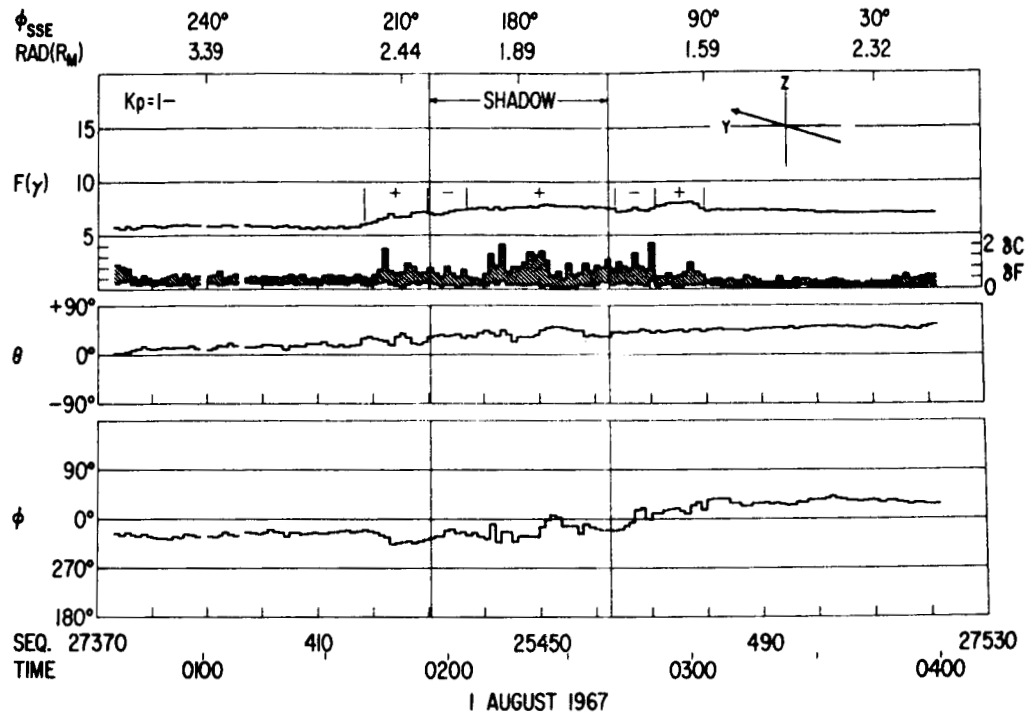
ϕ_{SSE} 240° 210° 180° 90° 30°
RAD(R_M) 3.39 2.44 1.89 1.59 2.32
Kp=1−
SHADOW
Z
Y
15
F(γ) 10
5
2 δC
δF
0
+90°
θ 0°
−90°
90°
φ 0°
270°
180°
SEQ. 27370 410 25450 490 27530
TIME 0100 0200 0300 0400
1 AUGUST 1967

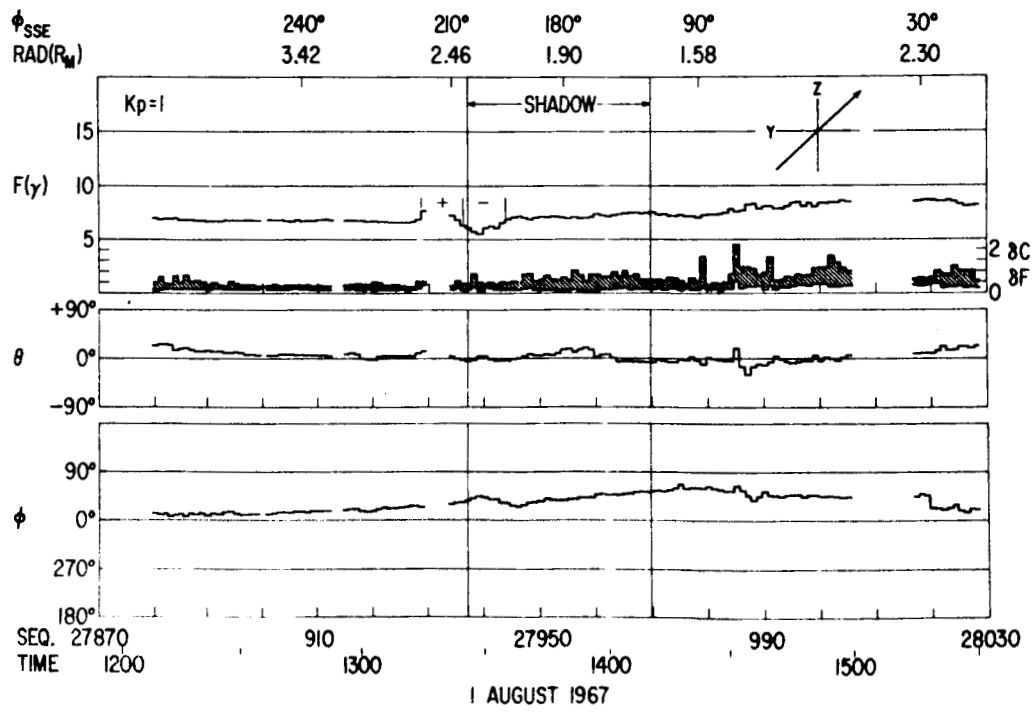
ϕ_{SSE} 240° 210° 180° 90° 30°
RAD(R_M) 3.42 2.46 1.90 1.58 2.30
Kp=1
SHADOW
Z
Y
15
F(γ) 10
5
2 δC
δF
0
+90°
θ 0°
−90°
90°
φ 0°
270°
180°
SEQ. 27870 910 27950 990 28030
TIME 1200 1300 1400 1500
1 AUGUST 1967

Figure 2

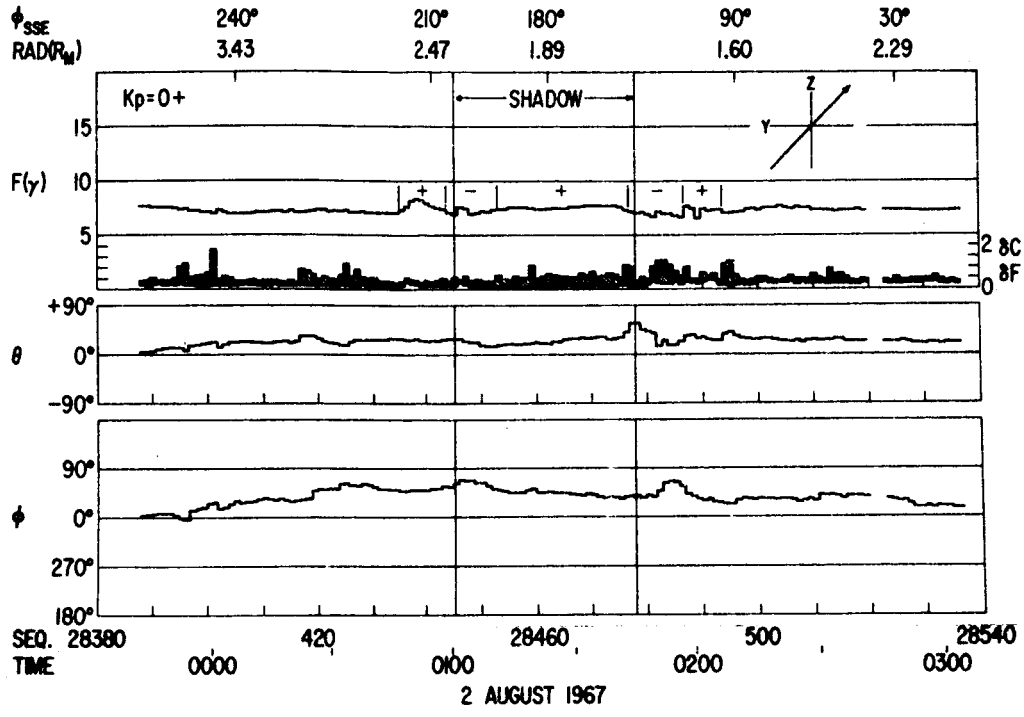
ϕ_{SSE} 240° 210° 180° 90° 30°
RAD(R_M) 3.43 2.47 1.89 1.60 2.29
Kp=0+
SHADOW
Z
Y
F(y)
15
10
5
2 δC
0 δF
θ
+90°
0°
-90°
φ
90°
0°
270°
180°
SEQ. 28380 420 28460 500 28540
TIME 0000 0100 0200 0300
2 AUGUST 1967

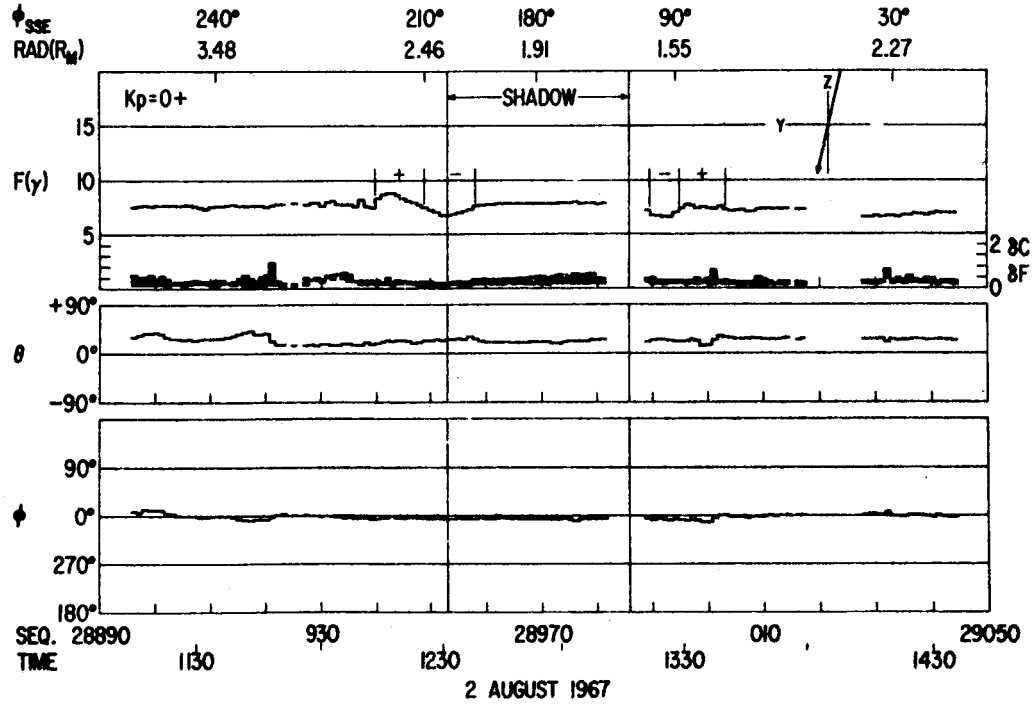
ϕ_{SSE} 240° 210° 180° 90° 30°
RAD(R_M) 3.48 2.46 1.91 1.55 2.27
Kp=0+
SHADOW
Z
Y
F(y)
15
10
5
2 δC
0 δF
θ
+90°
0°
-90°
φ
90°
0°
270°
180°
SEQ. 28890 930 28970 010 29050
TIME 1130 1230 1330 1430
2 AUGUST 1967

Figure 3

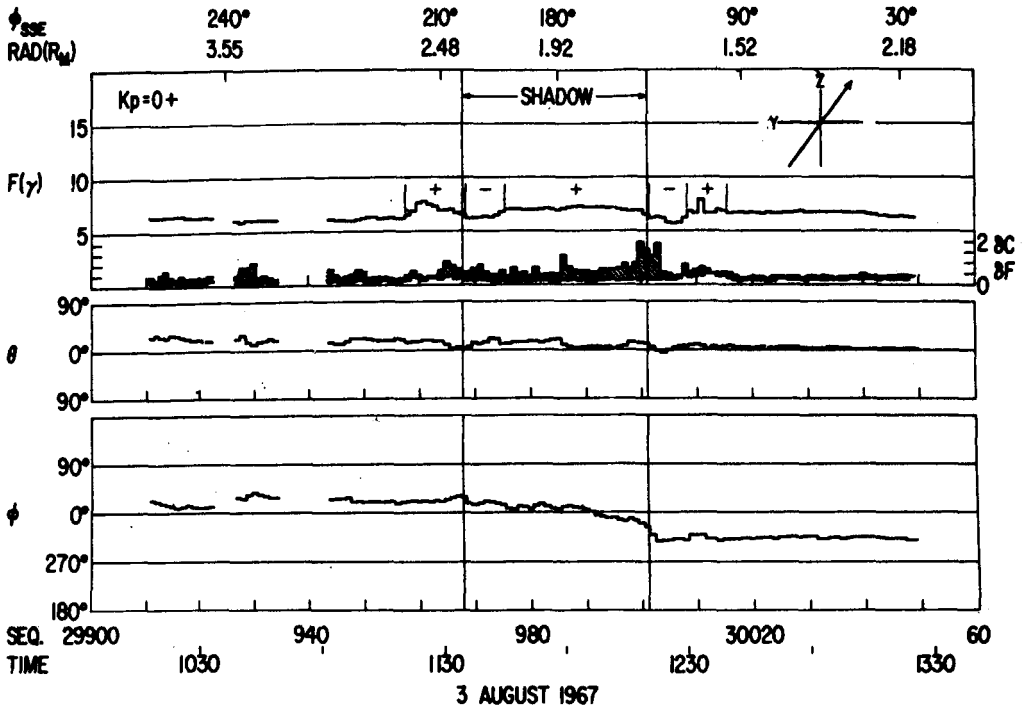
ϕ_{SSE} 240° 210° 180° 90° 30°
RAD(R_M) 3.55 2.48 1.92 1.52 2.18
Kp=0+
SHADOW
F(γ)
δC
δF
θ
φ
SEQ. 29900 940 980 30020 60
TIME 1030 1130 1230 1330
3 AUGUST 1967

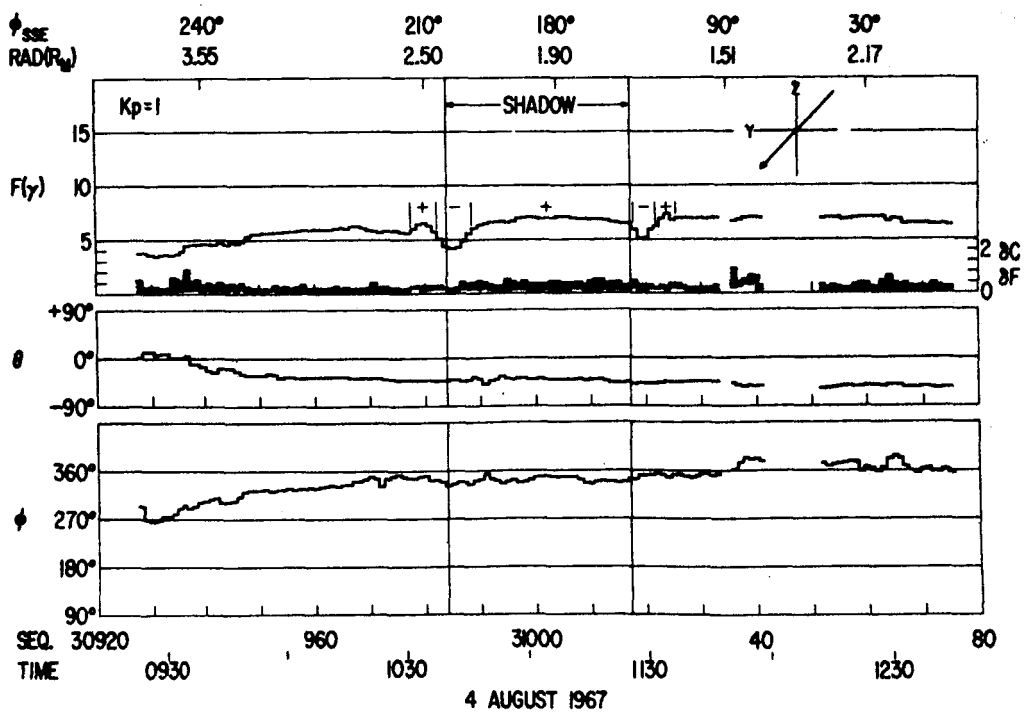
ϕ_{SSE} 240° 210° 180° 90° 30°
RAD(R_M) 3.55 2.50 1.90 1.51 2.17
Kp=1
SHADOW
F(γ)
δC
δF
θ
φ
SEQ. 30920 960 31000 40 80
TIME 0930 1030 1130 1230
4 AUGUST 1967

Figure 4

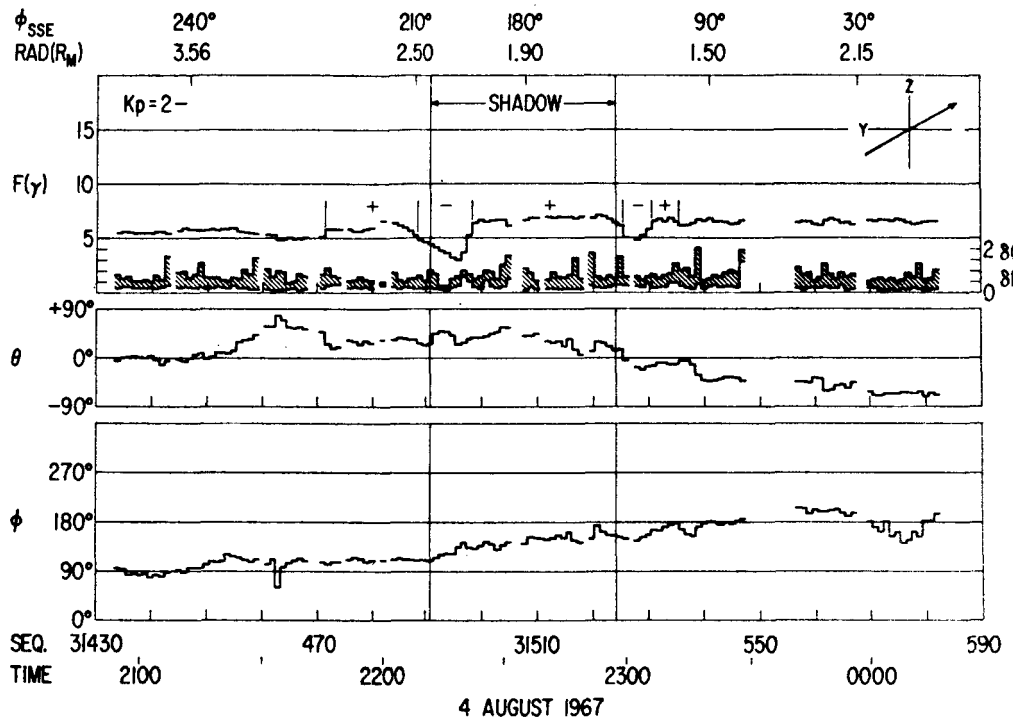
ϕ_{SSE} 240° 210° 180° 90° 30°
RAD(R_M) 3.56 2.50 1.90 1.50 2.15
Kp=2−
SHADOW
Z
Y
15
F(y) 10
5
2 δC
0 δF
+90°
θ 0°
−90°
270°
φ 180°
90°
0°
SEQ. 31430 470 31510 550 590
TIME 2100 2200 2300 0000
4 AUGUST 1967

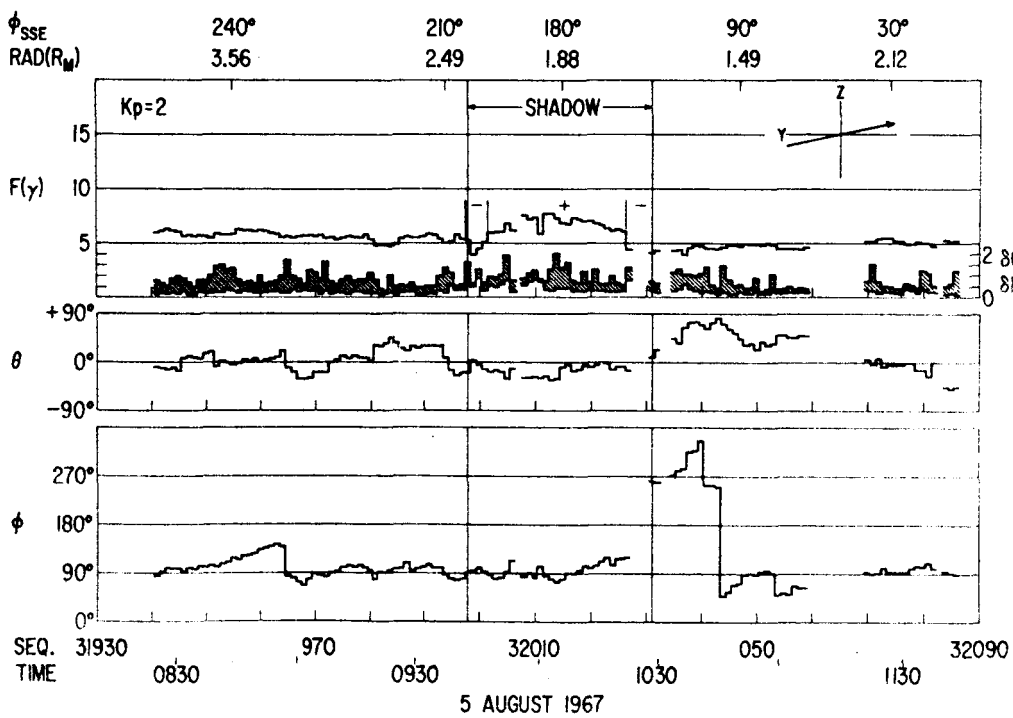
ϕ_{SSE} 240° 210° 180° 90° 30°
RAD(R_M) 3.56 2.49 1.88 1.49 2.12
Kp=2
SHADOW
Z
Y
15
F(y) 10
5
2 δC
0 δF
+90°
θ 0°
−90°
270°
φ 180°
90°
0°
SEQ. 31930 970 32010 050 32090
TIME 0830 0930 1030 1130
5 AUGUST 1967

Figure 5

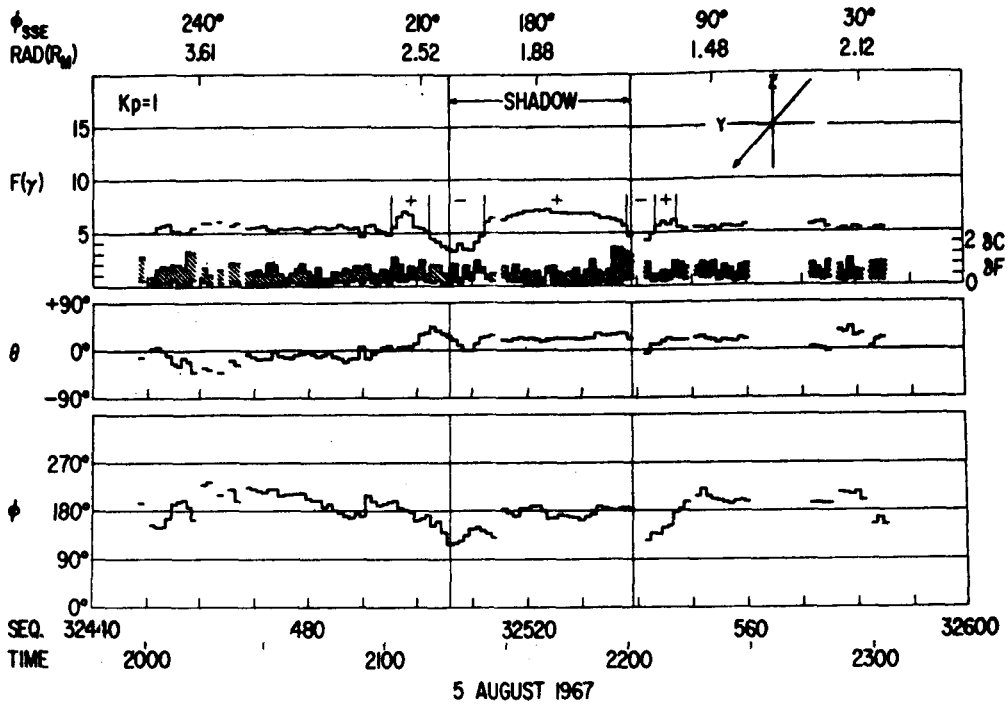
ϕ_{SSE} 240° 210° 180° 90° 30°
RAD(R_M) 3.61 2.52 1.88 1.48 2.12
Kp=1
SHADOW
Z
Y
15
F(γ) 10
5
2 δC
0 δF
+90°
θ 0°
-90°
270°
φ 180°
90°
0°
SEQ. 32440 480 32520 560 32600
TIME 2000 2100 2200 2300
5 AUGUST 1967

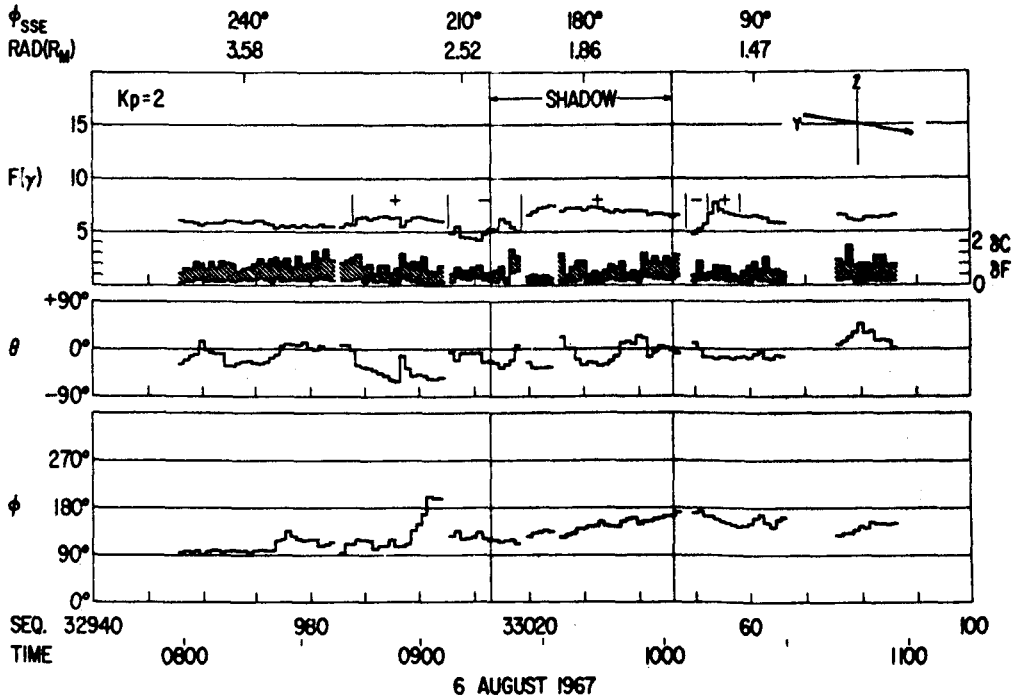
ϕ_{SSE} 240° 210° 180° 90°
RAD(R_M) 3.58 2.52 1.86 1.47
Kp=2
SHADOW
Z
Y
15
F(γ) 10
5
2 δC
0 δF
+90°
θ 0°
-90°
270°
φ 180°
90°
0°
SEQ. 32940 980 33020 60 100
TIME 0800 0900 1000 1100
6 AUGUST 1967

Figure 6

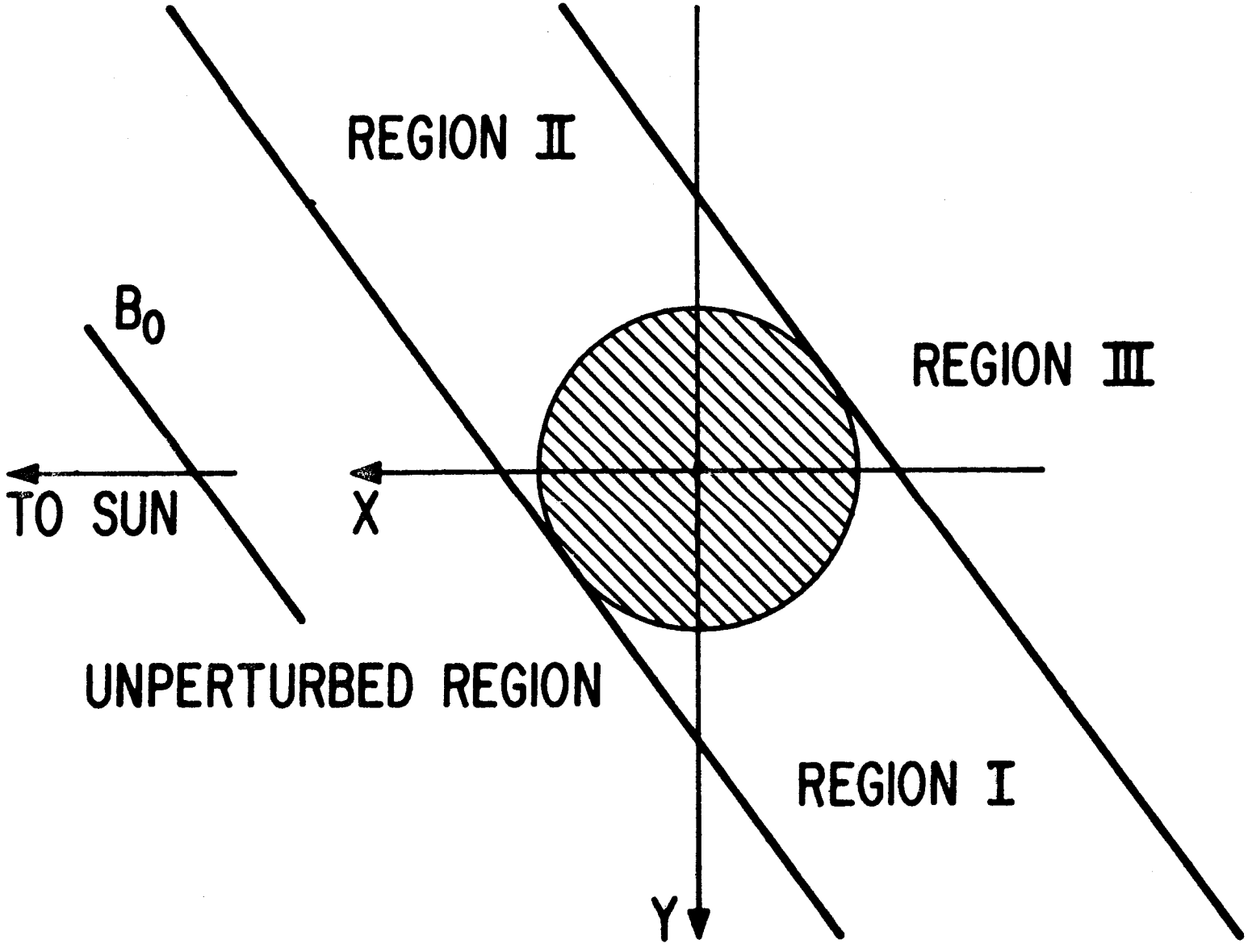
REGION II
B_0
REGION III
TO SUN
X
UNPERTURBED REGION
REGION I
Y

Figure 7

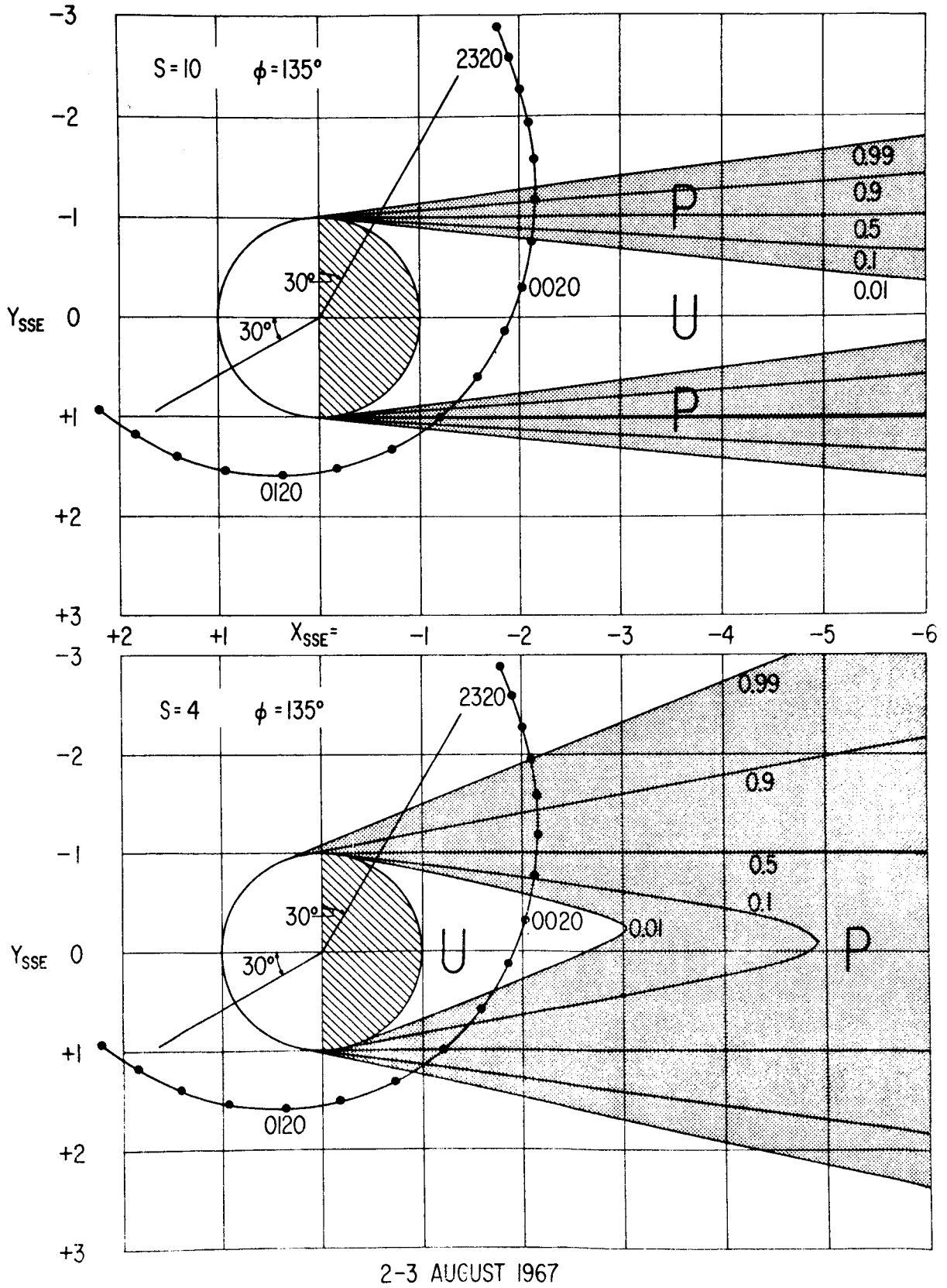
S = 10
φ = 135°
2320
0020
0120
30°
30°
0.99
0.9
0.5
0.1
0.01
P
U
P
Y_{SSE}
X_{SSE} =
-3
-2
-1
0
+1
+2
+3
+2
+1
-1
-2
-3
-4
-5
-6
S = 4
φ = 135°
2320
0020
0120
30°
30°
0.99
0.9
0.5
0.1
0.01
U
P
Y_{SSE}
2-3 AUGUST 1967

Figure 8

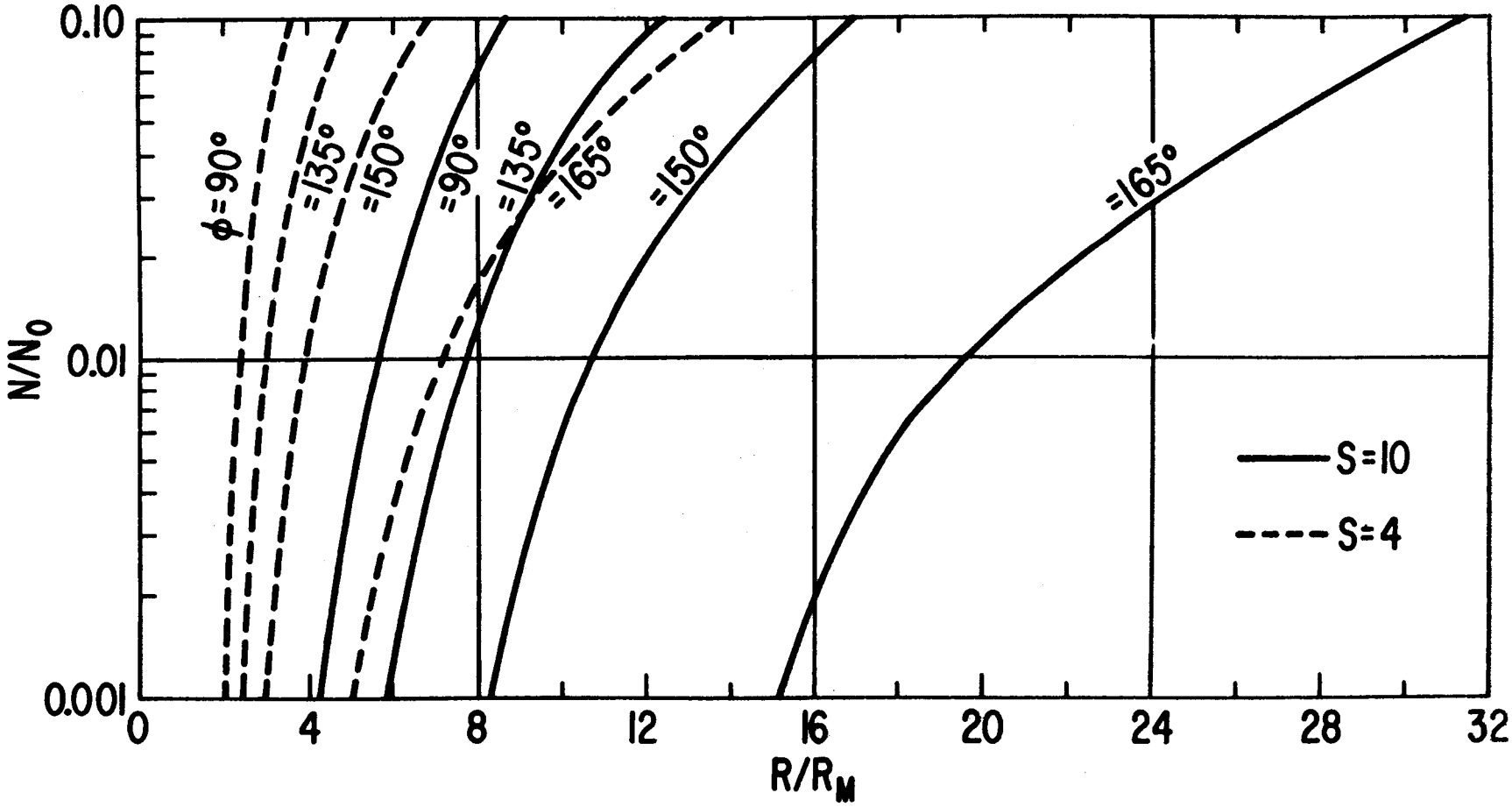
0.10
0.01
0.001
N/N0
0
4
8
12
16
20
24
28
32
R/RM
φ=90°
=135°
=150°
=90°
=135°
=165°
=150°
=165°
S=10
S=4

Figure 9

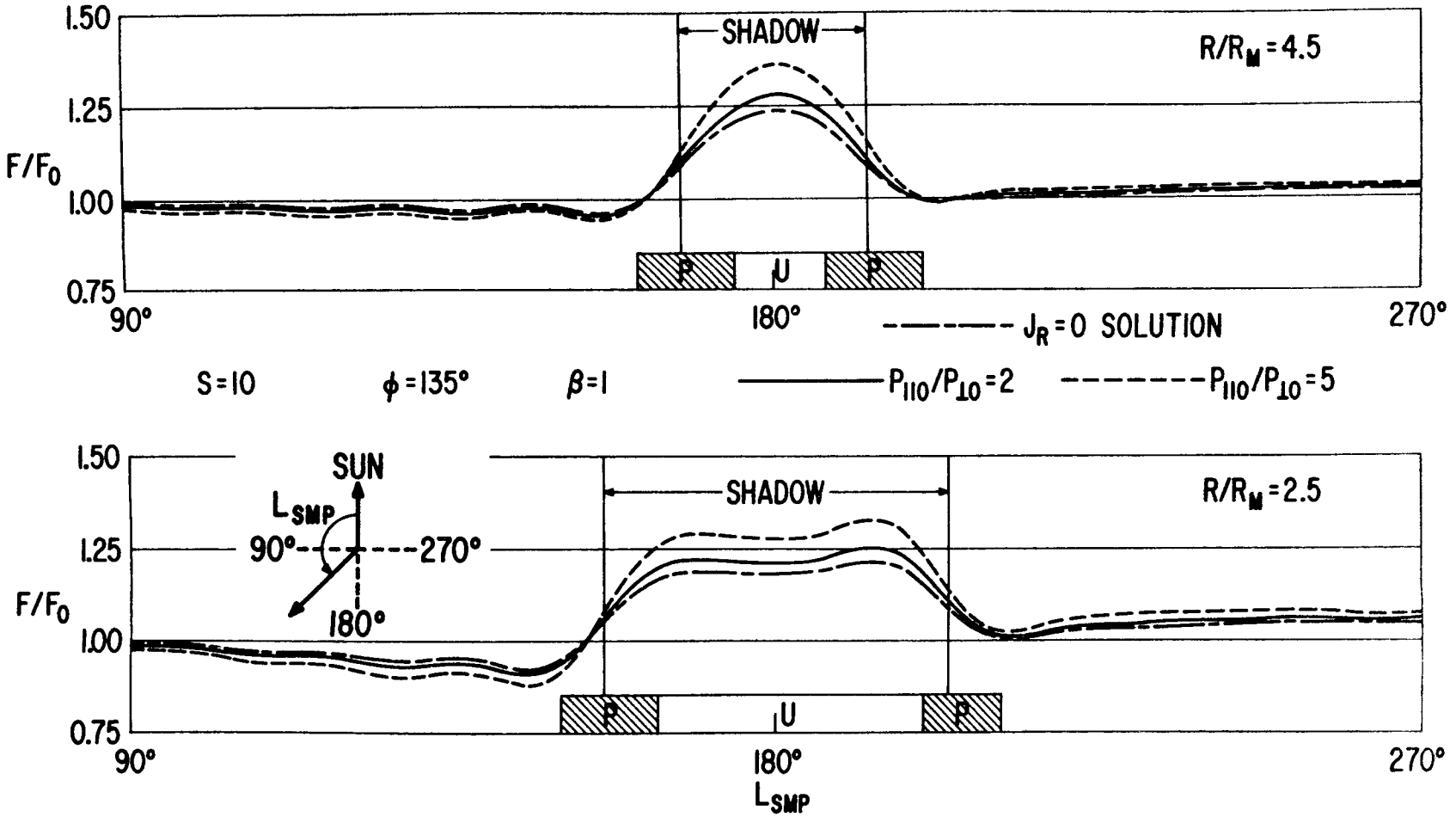
1.50
1.25
1.00
0.75
F/F0
SHADOW
R/RM=4.5
P
U
P
90°
180°
270°
JR=0 SOLUTION
S=10
φ=135°
β=1
P110/P⊥0=2
P110/P⊥0=5
SUN
LSMP
90°
270°
180°
R/RM=2.5

Figure 10

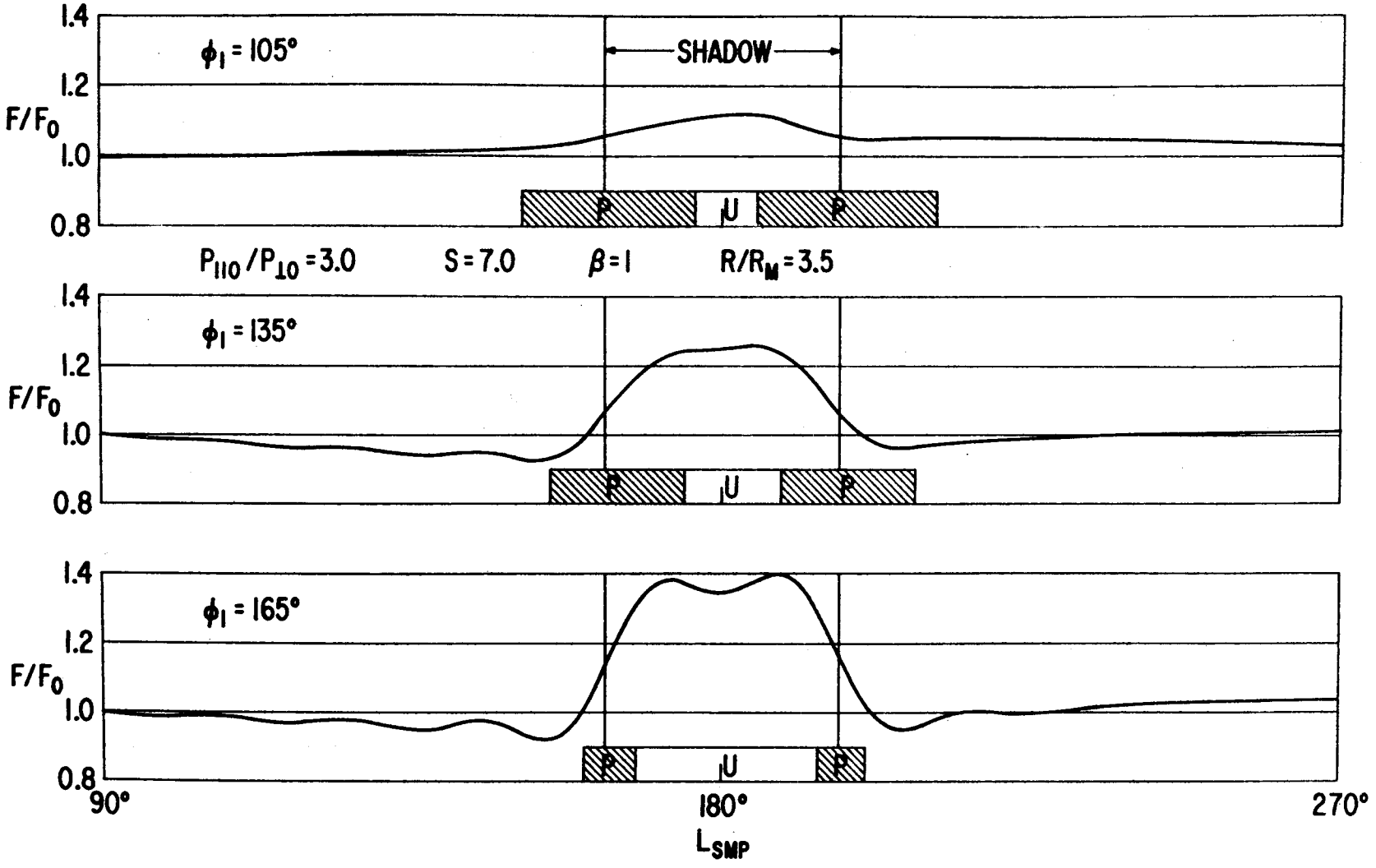
1.4
1.2
1.0
0.8
F/F0
ϕ1 = 105°
SHADOW
P
U
P
P110/P⊥0 = 3.0
S = 7.0
β = 1
R/RM = 3.5
ϕ1 = 135°
ϕ1 = 165°
90°
180°
270°
LSMP

Figure 11

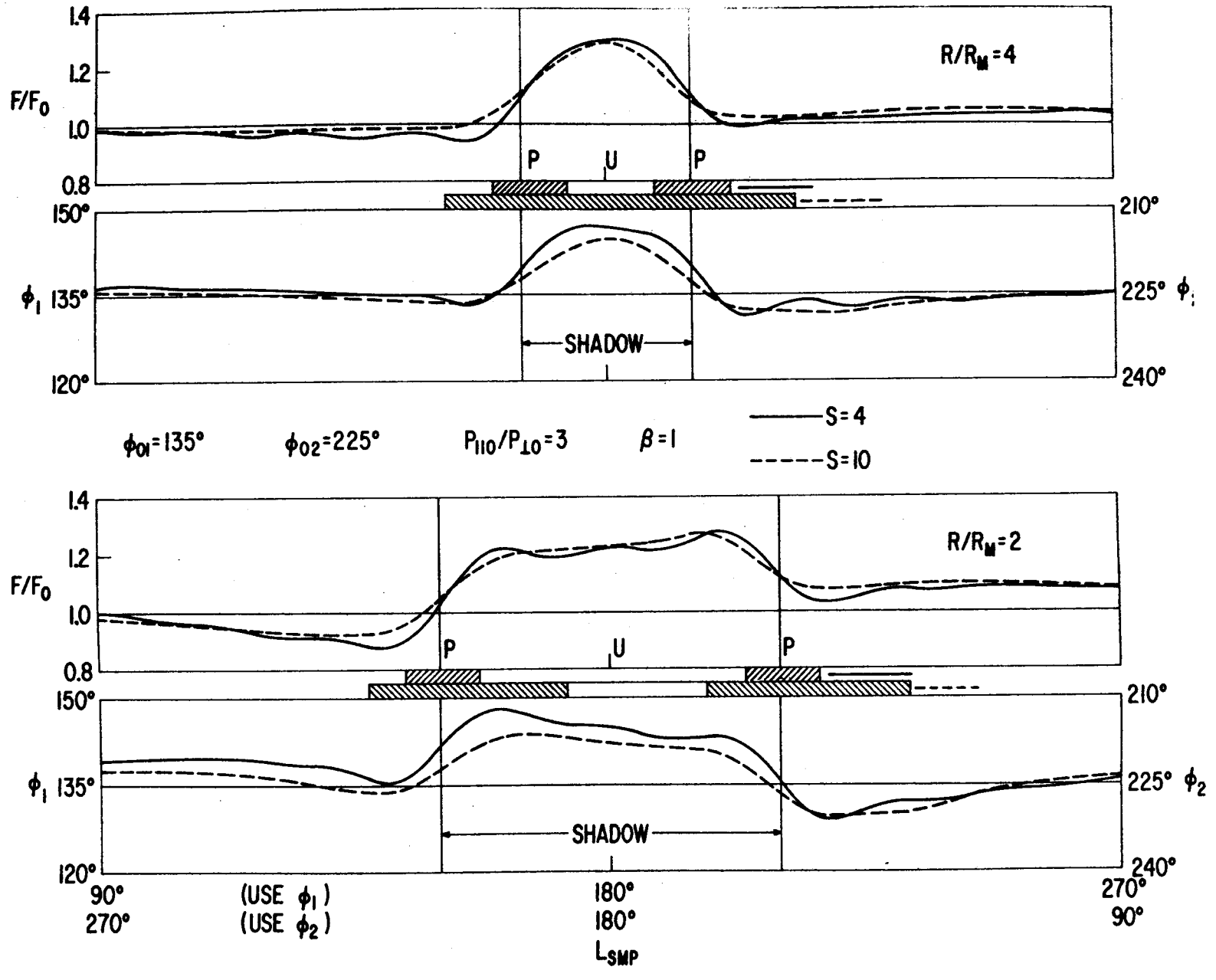
1.4
1.2
F/F0
1.0
0.8
R/RM=4
P
U
P
150°
210°
φ1 135°
225° φ2
SHADOW
120°
240°
φ01=135°
φ02=225°
P110/P⊥0=3
β=1
S=4
S=10
R/RM=2
90°
270°
(USE φ1)
(USE φ2)
180°
180°
LSMP

Figure 12

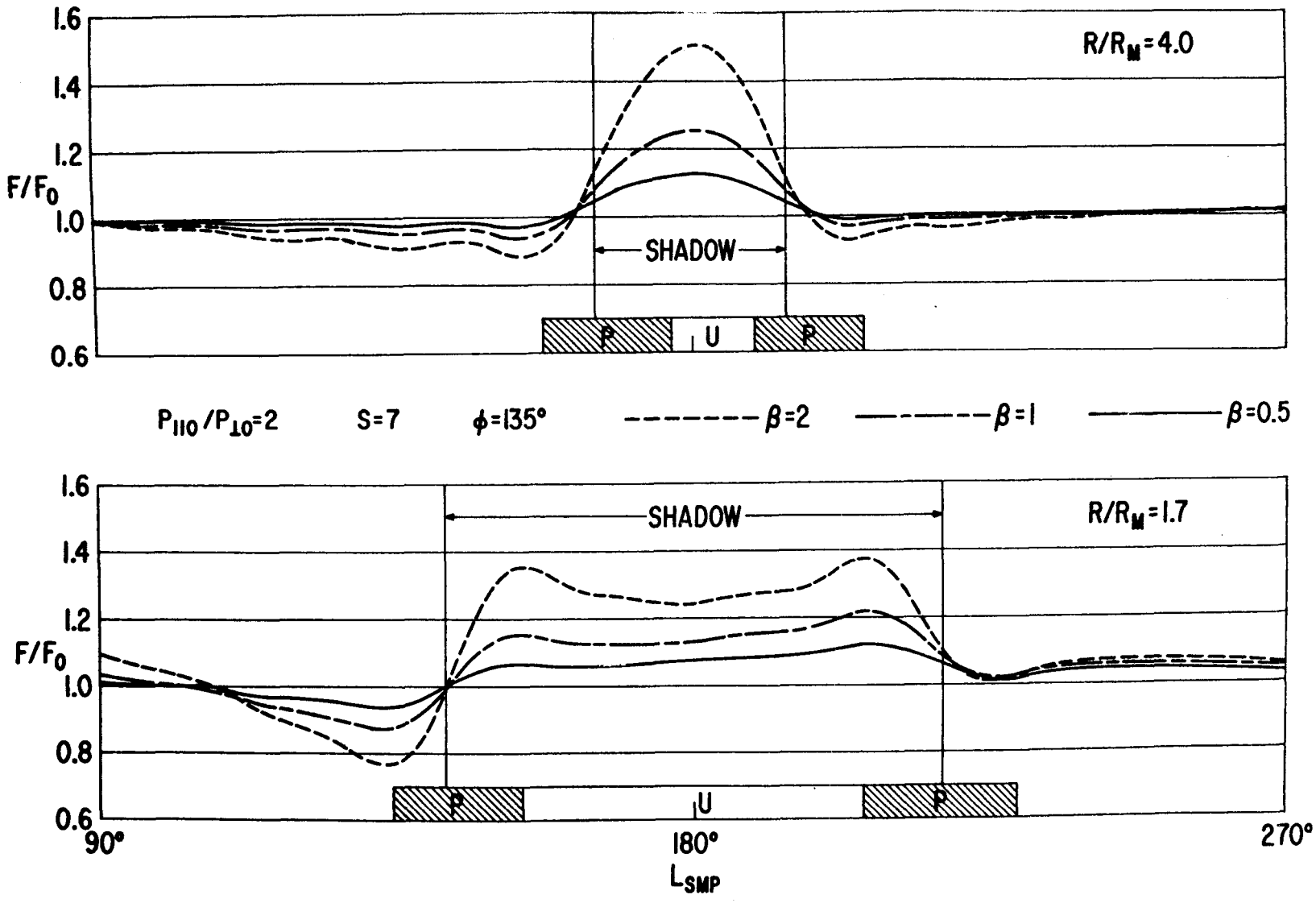
1.6
1.4
1.2
1.0
0.8
0.6
F/F0
R/RM=4.0
SHADOW
P
U
P
P110/P⊥0=2
S=7
φ=135°
β=2
β=1
β=0.5
1.6
1.4
1.2
1.0
0.8
0.6
F/F0
SHADOW
R/RM=1.7
P
U
P
90°
180°
270°
LSMP

Figure 13

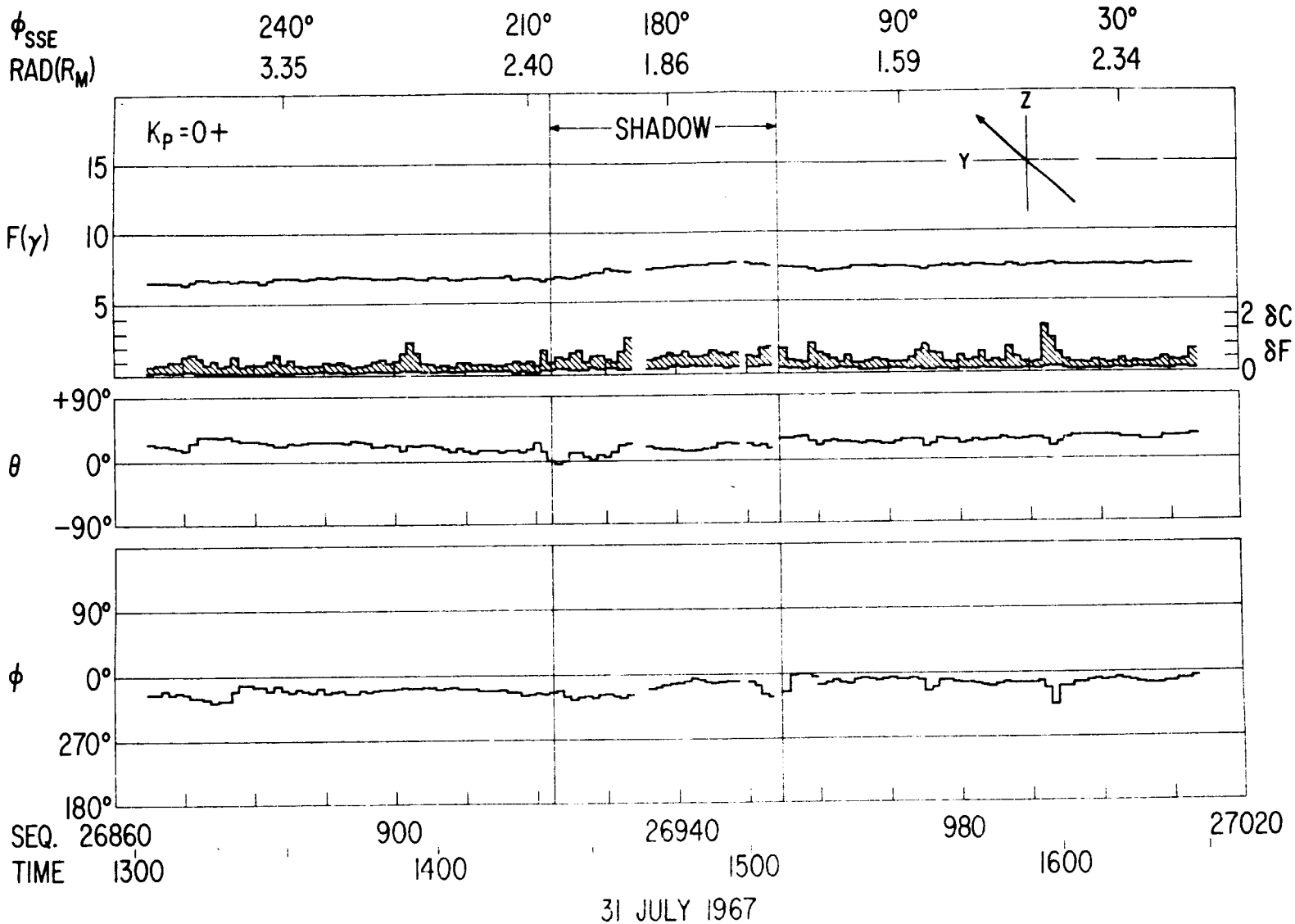
ϕ_{SSE}
240°
210°
180°
90°
30°
RAD(R_M)
3.35
2.40
1.86
1.59
2.34
K_p = 0+
SHADOW
Z
Y
15
F(γ)
10
5
2 δC
0
δF
+90°
θ
0°
-90°
90°
φ
0°
270°
180°
SEQ. 26860
900
26940
980
27020
TIME 1300
1400
1500
1600
31 JULY 1967

Figure 14